Marine Geology 427 (2020) 106221

Contents lists available at ScienceDirect

Marine Geology

journal homepage: www.elsevier.com/locate/margo

Continental slope and rise geomorphology seaward of the Totten Glacier, East Antarctica (112°E-122°E)

P.E. O'Brien[a,*], A.L. Post[b], S. Edwards[c], T. Martin[c], A. Caburlotto[d], F. Donda[d], G. Leitchenkov[e], R. Romeo[d], M. Duffy[f], D. Evangelinos[g], L. Holder[h], A. Leventer[f], A. López-Quirós[g], B.N. Opdyke[i], L.K. Armand[i]

[a] Department of Environmental Sciences, Macquarie University, Sydney, Australia
[b] Geoscience Australia, Canberra, Australia
[c] CSIRO Oceans and Atmosphere, Hobart, Australia
[d] Istituto Nazionale di Oceanografia e di Geofisica Sperimentale (OGS), Italy
[e] All-Russia Scientific Research Institute for the Geology and Mineral Resources of the Ocean St.- Petersburg, St.-Petersburg State University, St.-Petersburg, Russia
[f] Colgate University, NY, USA
[g] Instituto Andaluz de Ciencias de la Tierra, CSIC-Universidad de Granada, Avda. de las Palmeras 4, 18100 Armilla, Granada, Spain
[h] Imperial College, London, United Kingdom
[i] Australian National University, Canberra, Australia

ARTICLE INFO

Keywords:
Antarctica
Continental slope and rise
Totten Glacier
Submarine canyons
Ridges

ABSTRACT

The continental slope and rise seaward of the Totten Glacier and the Sabrina Coast, East Antarctica features continental margin depositional systems with high sediment input and consistent along-slope current activity. Understanding their genesis is a necessary step in interpreting the paleoenvironmental records they contain. Geomorphic mapping using a systematic multibeam survey shows variations in the roles of downslope and along slope sediment transport influenced by broad-scale topography and oceanography. The study area contains two areas with distinct geomorphology. Canyons in the eastern part of the area have concave thalwegs, are linked to the shelf edge and upper slope and show signs of erosion and deposition along their beds suggesting cycles of activity controlled by climate cycles. Ridges between these canyons are asymmetric with crests close to the west bank of adjacent canyons and are mostly formed by westward advection of fine sediment lofted from turbidity currents and deposition of hemipelagic sediment. They can be thought of as giant levee deposits. The ridges in the western part of the area have more gently sloping eastern flanks and rise to shallower depths than those in the east. The major canyon in the western part of the area is unusual in having a convex thalweg; it is likely fed predominantly by mass movement from the flanks of the adjacent ridges with less sediment input from the shelf edge. The western ridges formed by accretion of suspended sediment moving along the margin as a broad plume in response to local oceanography supplemented with detritus originating from the Totten Glacier. This contrasts with interpretations of similar ridges described from other parts of Antarctica which emphasise sediment input from canyons immediately up-current. The overall geomorphology of the Sabrina Coast slope is part of a continuum of mixed contourite-turbidite systems identified on glaciated margins.

1. Introduction

Studies of the Antarctic margin have shown that the continental slope and rise are the major sink for sediment removed from the continent for at least 34 Ma of episodic glaciation (Cooper and O'Brien, 2004). The expression of this long history on the slope and rise is an array of geomorphic features that have only been well documented in a few areas (e.g. Rebesco et al., 1996, Dowdeswell et al., 2006, Gales et al., 2013, Amblas and Canals, 2016, Larter et al., 2016). Where the Antarctic slope and rise have been well studied, their geomorphology reflect high sediment input from the continent and persistent along slope current activity producing a set of deposits included in the facies model for contourites (Rebesco et al., 1996). The Antarctic slope and rise are important sites for recovery of paleoclimate records so understanding depositional processes are an essential step in deciphering climate history. In addition, understanding Antarctic margin

* Corresponding author.
E-mail address: phil.obrien.ant@gmail.com (P.E. O'Brien).

https://doi.org/10.1016/j.margeo.2020.106221
Received 10 July 2019; Received in revised form 30 April 2020; Accepted 4 May 2020
Available online 20 May 2020

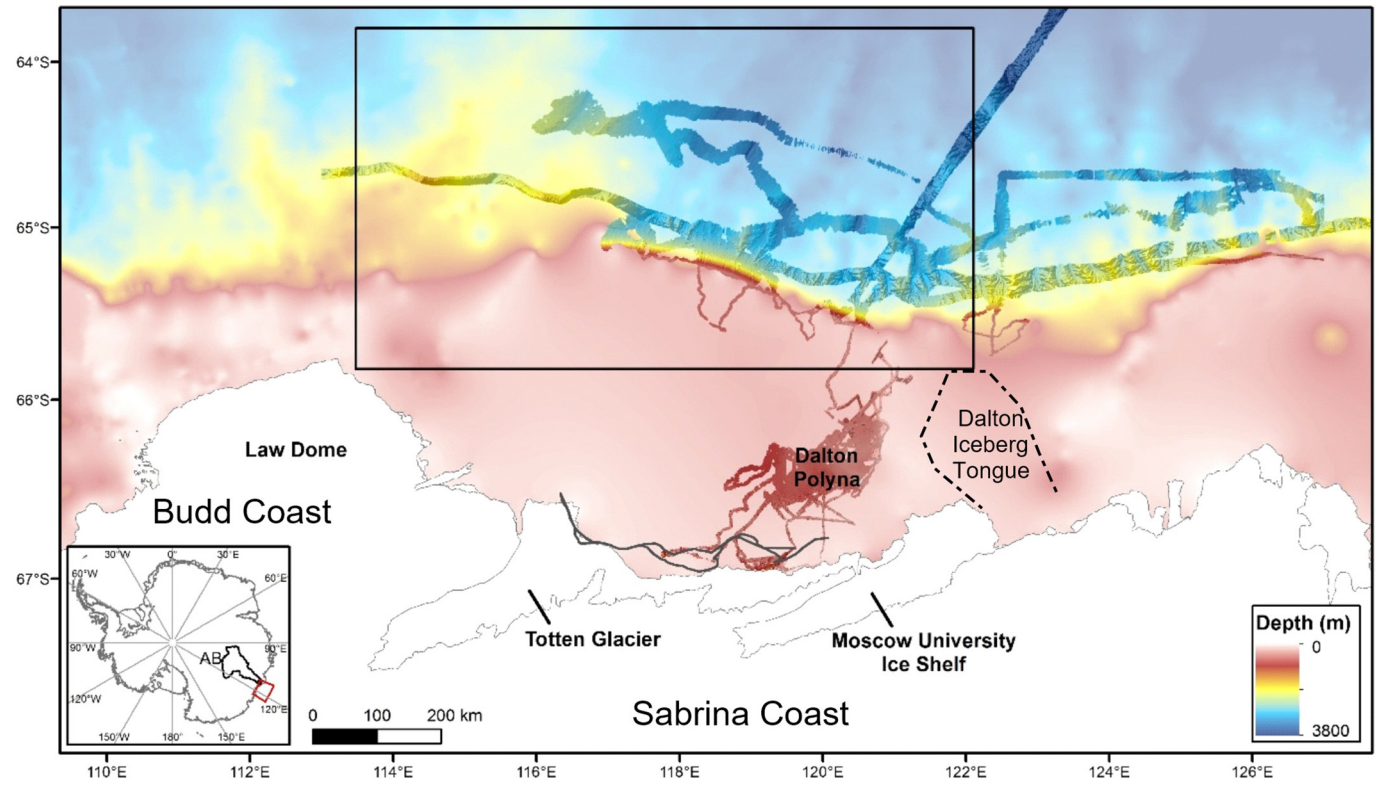

a.

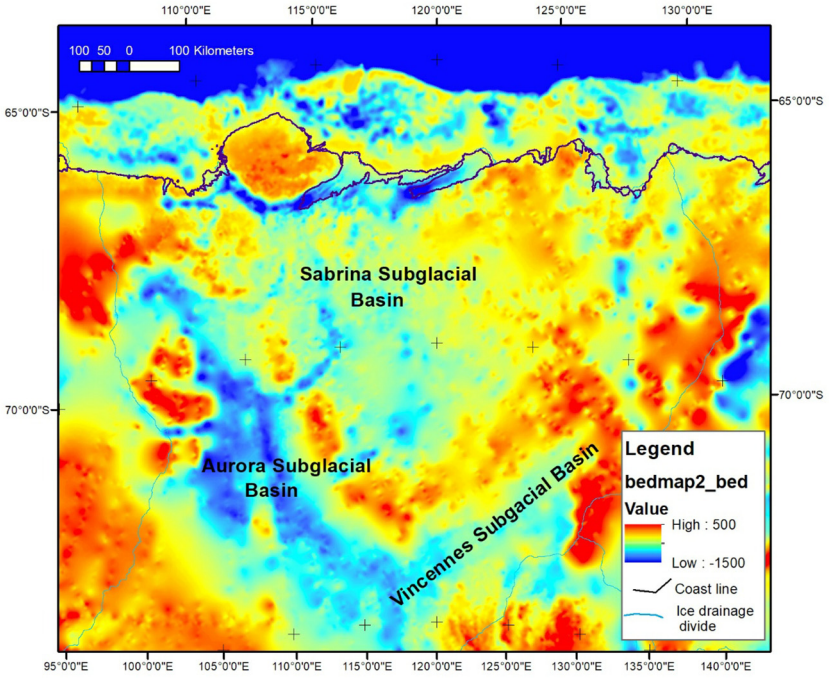

b.

Fig. 1. a. Location of study area with major glaciological features for the Budd and Sabrina Coasts. Bathymetry is from the International Bathymetric Chart of the Southern Ocean (IBSCO, Arndt et al., 2013). Darker swaths are from two surveys by the *Nathaniel B Palmer* (NBP1402, NBP1503, Nitsche et al., 2017, Fernandez et al., 2018). Single track is from a single beam survey by the *RV Aurora Australis* (Rintoul et al., 2016). b. Subglacial topography in the hinterland of the study area showing subglacial basins after Aitken et al. (2016). Elevations from BEDMAP2 (Fretwell et al., 2013). Ice drainage divides from NASA (http://icesat4.gsfc.nasa.gov/cryo_data/ant_grn_drainage_systems.php).

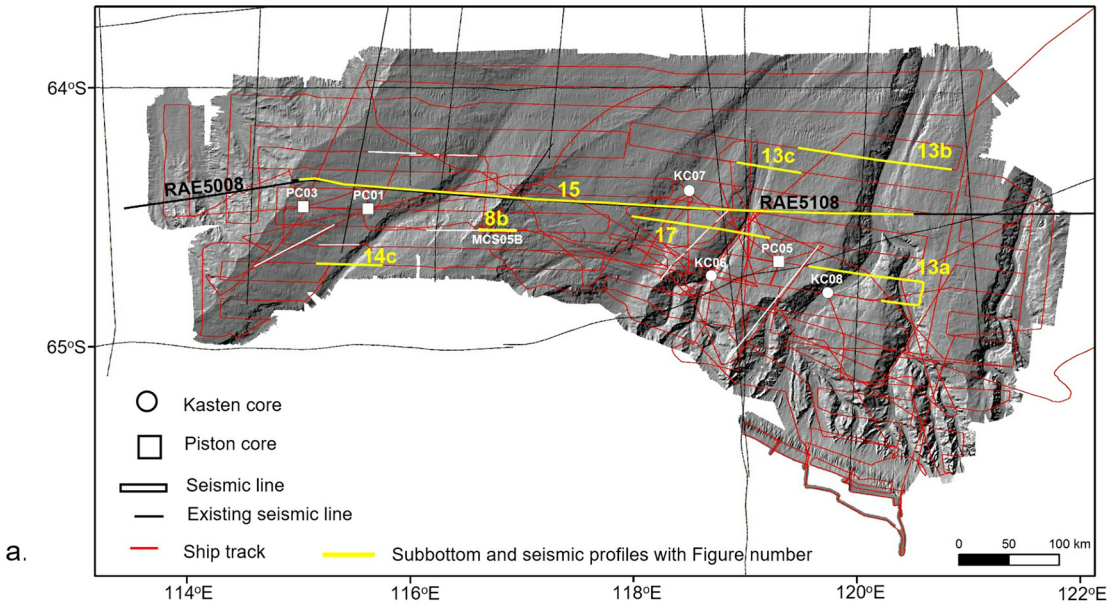

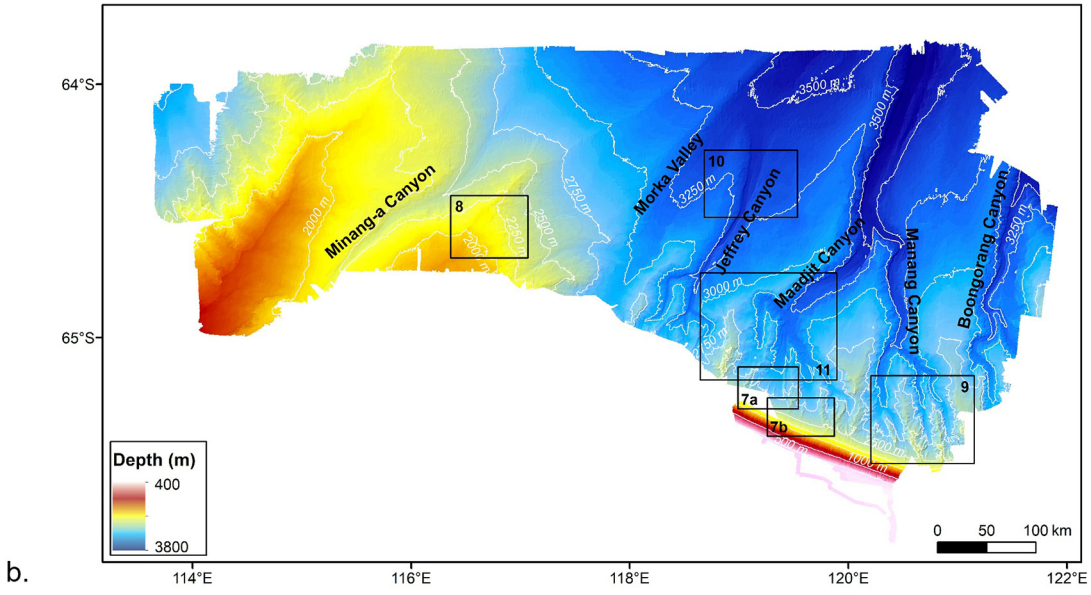

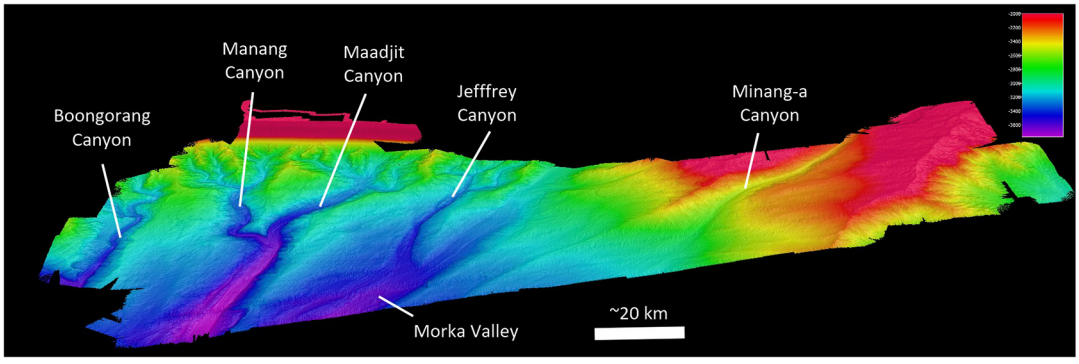

Fig. 2. a. Multibeam data, ships tracks, core sites and seismic lines for survey IN2017-V01 (Sabrina Sea Floor Survey) as well as existing seismic lines for the survey area. Cores and seismic lines mentioned in the paper are labelled. Background image is a shaded greyscale image of the multibeam data collected during the survey. b. Panchromatic rendition of the IN2017-V01 multibeam bathymetry with proposed canyon names and boxes showing location of other figures in this paper. c. Fledermaus 3-D image of the multibeam bathymetric grid viewed from the NNW. Canyon names indicated.

sedimentation can shed light on other settings with high sediment input and lateral current activity, including margins where ancient deposits have resource potential (e.g. Fonnesu et al., 2020).

The East Antarctic margin is particularly important because it reflects the history of the longest-lived ice sheet on earth which is also the largest ice mass at present. Previous studies have relied mostly on single beam bathymetry and seismic reflection profiles (Kuvaas and Leitchenkov, 1992, Escutia et al., 2000) with multibeam coverage of the Antarctic Peninsula and George V Land margins (Rebesco et al., 2007, Amblas and Canals, 2016, Beaman et al., 2011). Areas seaward of large outlet glaciers of the East Antarctic Ice Sheet have not been surveyed with multibeam. These large outlet glaciers are potential barometers of wider ice sheet behaviour and points of vulnerability to warming climate (Pritchard et al., 2012). One of these is the Totten Glacier which flows through the Sabrina Coast between 112°E and 120°E. It drains a substantial inland basin (Aitken et al., 2016) and has shown rapid thinning in recent years (Pritchard et al., 2012). This paper presents multibeam data and geomorphic mapping of an area covering a major slope depocenter seaward of the Totten Glacier and the smaller drainage features to the east.

Surveys of the sea floor seaward of outlet glaciers can be used to understand ice behaviour and mapping and dating of sea floor landforms on the shelf can indicate how rapidly the glacier retreated after the Last Glacial Maximum (LGM) (e.g. O'Cofaigh et al., 2008; Macintosh et al., 2011; Smith et al., 2011; Fernandez et al., 2018). The continental slope and rise provide additional insights by preserving more complete records covering multiple glacial cycles in places (e.g. Levy et al., 2019), whereas the shelf typically retains only the post-LGM record. The addition of biogenic sediment to slope and rise successions provides potential for dating and paleoenvironmental study. Sediments on the continental slope can record timing of multiple ice advances and retreats and contain evidence of the oceanic water masses in contact with the sediments and the ice during these episodes (Weber et al., 2011).

Studies of rapidly retreating outlet glaciers in the Amundsen Sea have shown a major role for a warm water mass known as Modified Circumpolar Deep Water (MCDW), which flows onto the shelf from the deep ocean and enhances melting (Jenkins et al., 2010; Smith et al., 2011; Pritchard et al., 2012). This process has also been suggested as a cause of rapid melting of the Totten Glacier (Pritchard et al., 2012; Williams et al., 2011). Pritchard et al., (2012) invoke changes in the circum-Antarctic wind field and its effects on upwelling around the continent as the cause of Totten Glacier rapid basal melting. Gwyther et al. (2014) and Khazender et al. (2013) argue that this enhanced melting is the result of complex interactions between oceanic and shelf water masses with the base of the ice. They suggest that the melting is strongly modulated by cold High Salinity Shelf Water formed in polynyas to the east of the Totten Glacier and channelled by local bathymetry to the base of the glacier. These studies rely heavily on satellite observations and bathymetry of the regions.

While past research on paleoclimate archives from the Antarctic slope and rise have been fruitful (e.g. Weber et al., 2011; Levy et al., 2019), slope sedimentation is not uniform and both the choice of sample sites and the interpretation of recovered sections should be informed by knowledge of the local depositional setting and processes active in the area. The ridges overlying thick sedimentary sequences seaward of the Amery Ice Shelf and Totten Glacier have been examined with wide-spaced seismic lines but do not have dense bathymetric coverage so that understanding of the surface processes shaping their morphology is limited. This study uses a systematic multibeam survey to enhance the understanding of East Antarctic slope and rise sedimentation for paleoclimate interpretation and to add to the overall understanding of continental margin sedimentation where both downslope and along-slope processes interact.

In early 2017, the Sabrina Seafloor Survey set out to map the continental margin seaward of the Sabrina Coast of East Antarctica with the aim of improving understanding of the long-term behaviour of the Totten Glacier. The survey took place on the Australian Marine National Facility vessel *R.V. Investigator* (Survey number IN2017-V01). The study area was first systematically surveyed with multibeam echo sounders and subbottom profiler (Figs. 1, 2a). These data have been used to map the geomorphology of the slope and rise in order to understand local sedimentary processes as a precursor to interpreting the sediment cores. In addition, high resolution multichannel seismic lines and oceanographic observations were collected. Examination of regional bathymetry compilations shows that the study area includes continental slope similar to other parts of the East Antarctic margin but also covers a relatively shallow ridge (Fig. 1). Close et al. (2007) estimated around 7 km of sediment younger than the onset of Antarctic glaciation in a depocentre corresponding to this ridge.

1.1. Location

The study area is on the Antarctic continental slope and rise between 113° 30′E and 122°E and covering latitudes from 63° 48′S to 65° 36′S (Fig. 1a). The area is seaward of the Budd and Sabrina Coasts of Wilkes Land. Water depths surveyed vary from 450 m on the shelf to 3747 m in canyons at the northern edge of the area. The area was chosen to target deposits seaward of major glaciological features in the region. Recent multibeam surveys (Fernandez et al., 2018; Nitsche et al., 2017), and a single beam transect along the front of the Totten Glacier (Rintoul et al., 2016) show that the shelf has overall geometry typical of Antarctica with a shelf edge at around 450–550 m and deepening towards the coast, reaching over 1000 m (Fig. 1). This bathymetry suggests the presence of deep troughs crossing the shelf from the Moscow University Ice Shelf and the Totten Glacier. Previous data compilations (IBSCO, Arndt et al., 2013) from the continental slope and rise show a series of canyons and ridges which shallow from east to west with the western ridges as shallow as 2000 m in mid slope.

The major coastal features of the East Antarctic Ice Sheet landward of the study area, from west to east are Law Dome, Totten Glacier and the Moscow University Ice Shelf (Fig. 1). Totten Glacier and Moscow University Ice Shelf are the seaward end of an extensive glacial drainage system (Zwally and Giovinetto, 2011). Aitken et al. (2016) used geophysical and ice radar data to identify a complex of subglacial topographic basins separated by narrow highlands (Fig. 1b). The Sabrina Subglacial Basin is the subglacial basin immediately landward of the Totten Glacier and Moscow University Ice Shelf. Further inland, the Aurora Basin connects to the Sabrina Subglacial Basin through valleys cut in subglacial ridges and connects further inland to the Vincennes Subglacial Basin. The region features an extensive subglacial drainage network connecting the ice divide with the margin which likely funnels subglacial meltwater from 287,000 km^2 of the East Antarctic Ice Sheet through the Totten Glacier to the ocean (Wright et al., 2012). This subglacial topography suggests that rapid retreat of the Totten Glacier grounding line into the continent could contribute at least 3.5 m of sea level rise (Greenbaum et al., 2015).

On the continental shelf, seaward of the eastern part of the Moscow University Ice Shelf, a dense concentration of grounded icebergs extending across shelf is known as the Dalton Iceberg Tongue. The presence of these grounded icebergs contributes to the formation of a persistent polynya on their western side known as the Dalton Polynya (Fig. 1).

From a geological point of view, this part of the East Antarctic continental margin is extensional, formed by rifting in the Late Jurassic with break up in the Santonian-Campanian (Close et al., 2007). The continental slope is underlain by the Budd Coast Basin which contains a thickness of about 9 km of post-rift sediments (Close et al., 2007). Close et al. (2007) and Donda et al. (2007) studied the broad sedimentation patterns and history along this part of the Antarctic margin. Close et al. (2007) mapped a major post-rift depocenter beneath that includes the western ridges. They noted its position downstream from the Totten Glacier suggesting that the depocenter was the sink for sediment

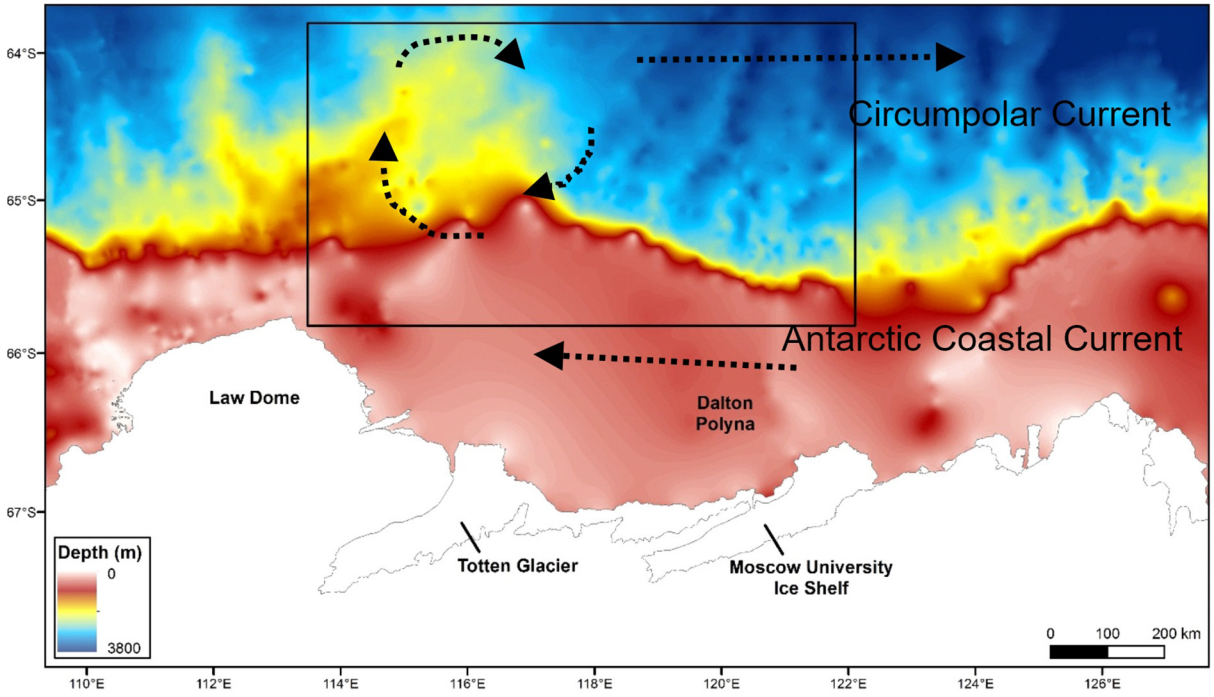

Fig. 3. Major ocean currents in the study area including the location of the Gyre identified by Wakatsuchi and Ohshima (1994).

derived from the Aurora Basin. Donda et al. (2007) interpreted the major phase of margin sedimentation as Miocene in age. This association with the downstream end of the Totten Glacier suggests that the ridges in the western part of the study area originated from extra sediment supply coming from the Totten Glacier, compared to those in the east which received sediment from smaller drainage basins.

The large-scale oceanographic features of the study area are described in Bindoff et al. (2000) and Williams et al. (2011). Water masses identified are Antarctic Surface Water (ASW), mostly on the shelf, Modified Circumpolar Deep Water (MCDW) and Antarctic Bottom Water (AABW), which comprises westward-flowing Adélie Land Bottom Water. The study area is mostly south of the Antarctic Circumpolar Current (ACC) and is dominated by the westward flowing Antarctic Coastal Current on the shelf and the Antarctic Slope current between 750 m and 1250 m on the slope, though Bindoff et al. (2000) identify a NW component of flow in the northern part of the study area (Fig. 3). Wakatsuchi and Ohshima (1994) interpreted three cyclonic gyres in the Southern Ocean around East Antarctica. Their Gyre I occurs in the study area with its northward leg along the western side. They suggest the gyres are controlled by sea floor ridges on the western side of the study area which deflect the westward-flowing Antarctic Coastal Current northward where water then encounters the east-flowing ACC (Fig. 3).

2. Data and methods

2.1. Data sources

The importance of the Totten Glacier and the basins it drains in understanding ice sheet behaviour and sea level change is such that a series of multinational research programs are under way. An airborne geophysical program has been mapping the geometry of the bed of the ice sheet that drains into the Totten Glacier (Young et al., 2011) and marine surveys have collected data on the shelf and slope. Of most value for this study are the multibeam bathymetry data collected by the US NSF vessel the *Nathaniel B. Palmer* on the continental shelf in the Dalton Polynya in early 2014 (Fernandez et al., 2018) and on the slope during survey NBP1503 in 2015 (Nitsche et al., 2017). Survey NBP1503 collected multibeam tracks in the study area but were unable to achieve full coverage because of heavy pack ice. They were able to acquire single tracks close to the shelf edge in areas inaccessible to the *RV Investigator* during this study.

Most of the data used in this study were collected during January–March 2017 on the Australian research vessel *RV Investigator*. Details of the survey are available at the Australian Marine National Facility web site under the survey number IN2017-V01 (https://www.cmar.csiro.au/data/trawler/survey_details.cfm?survey=IN2017_V01, Armand et al., 2018).

2.2. Bathymetry

Bathymetry was acquired using two multibeam echosounders, a Kongsberg EM122 and an EM710. The EM122 is a 12 kHz full ocean depth multibeam echosounder and was operated at all depth ranges on the Sabrina Seafloor Survey. The EM710 is a high resolution 70-100KHz sounder used for mapping on the continental shelf and upper slope to depths of up to 2000 m. The area was initially surveyed with East-West lines approximately 11 km apart (Figs. 1, 2a multibeam coverage). Some parts of the area could not be covered by the systematic grid because of sea ice however multibeam data collection continued throughout the survey to minimise data gaps.

Sound velocity corrections were undertaken using observed data from CTDs and eXpendable BathyThermographs (XBTs) as required. Observations of sea surface temperature were also used to construct profiles within SVP builder. Multibeam data were logged in Kongsberg's proprietary *.all format and were converted and processed within Caris HIPS and SIPS version 9.1.9. Raw files were generally converted into the HIPS and SIPS format using the batch processor, which after conversion loaded a zero-tide, computed Total Propagated Uncertainty (TPU) and merged the lines. A bathymetry filter was set up to reject beams outside a 65° angle from nadir. The data was then gridded at the highest resolution possible and further inspected for outliers and cleaned within the subset editor.

A swath angle surface at 50 m resolution was used as the working surface. Upon departure from the survey area final processing and QC of the data were undertaken. CUBE (Combined Uncertainty and Bathymetry Estimator) surfaces were generated at an appropriate

resolution for the depth, surface filters were then used extensively to automate noise reduction and outliers that remained present on the surface. The final surface was gridded at a resolution of 200 m, with a 50 m grid on the upper slope. The EM710 data on the shelf and upper slope were gridded to 10 m. The output surfaces were exported as ASCII and geotif files.

The Depth (CUBE) grids were imported into ArcGIS and the raster displayed as shaded relief images. A panchromatic sharpened image was also prepared using the ESRI algorithm in ArcMAP. Further rasters of slope magnitude and flow direction were produced using ArcGIS Spatial Analysis tools.

Canyon thalweg profiles were constructed using ArcGIS by running an Interpolated Line joining the deepest parts of each canyon and a Profile Graph produced. The submarine canyons on this slope are large valleys that merge with sediment ridges so we confine canyon widths and depths to the part of the active canyon valley similar to the Axial Incision of Baztan et al. (2005). Canyon Width-Depth ratios (W/D) were calculated by plotting an interpolated line on the bathymetric surface raster then making a profile graph using the tool in ArcGIS. The canyon width was estimated by picking a break in slope on each canyon side that represents the change from ridge flank to canyon wall (Fig. 4). Where the breaks in slope on either side were at different depths, the deepest depth was taken as the upper depth limit of the canyon. This depth was subtracted from the deepest depth on the canyon floor on the profile to give the canyon depth. The width was taken as the distance between the canyon side points. Canyon cross section shapes were quantified using the General Power Law program (Pattyn and Van Huele, 1998), which calculates the cross-sectional shape (b) by determining the minimum RMS (Root Mean Squared) between the observed cross-section and a large set of symmetrical shapes. A value of $b < 1$ indicates a convex-upward slope and a V-shaped profile, while $b > 2$ reflects a more box-shaped profile or U-shaped profile.

Canyon sinuosity was calculated by measuring the distance along a canyon thalweg and dividing this by the length of a straight line joining the beginning and end of the canyon in question.

The bathymetry grid was further examined using ArcGIS Hydrology tools. Grids of slope (Fig. 5) slope direction and flow accumulation, flow length and stream order were calculated. Normally, such analyses include steps to eliminate closed depressions and reverse gradients. These steps were not carried out on these data because there is no prima facie reason why closed basins and reverse gradients should not exist in the area. Visual examination of the grid images suggests the presence of slump structures and deposits which would disrupt normal drainage patterns in a terrestrial context so that applying processing steps that force drainage networks onto the data seemed inappropriate. The bathymetric grid was also imported into Fledermaus software for display as three-dimensional images with various vertical exaggerations and from different angles (Fig. 2c).

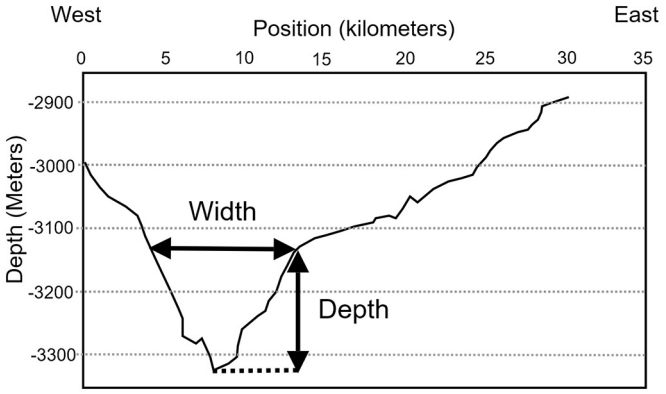

Fig. 4. Criteria used for Canyon width/depth (W/D) calculations. The canyon depth (D) is measured from the deepest point to a break in slope on the canyon side that best reflects a change from a confined valley to the adjacent ridge and the width (W) is measured at the depth of that break in slope.

2.3. Subbottom profiler

Subbottom profile data were acquired with a Kongsberg SPB120. On this voyage the system source was a linear chirp with a sweep of 2.5–6.5 kHz. The pulse length was 6 milliseconds and up to 12 milliseconds on transit through deep water. In the survey area the system operated in single ping mode but with burst during transit in deep water. A gain of 6 dB was applied to the data followed by gain correction, matched filter, instant amplitude processing and a time variable gain to enhance sub-bottom reflections. The sub-bottom profiler data was recorded and presented as two-way time sections. The subbottom profiles were saved as segy (Society of Exploration Geophysics Y format) and Kongsberg proprietary.raw files. Segy files were viewed in Seisee which allows adjustment of axes. The files were then exported as bmp files with the day and time along the horizontal axis and the two-way time along the vertical axis. All lines were numbered sequentially from the start to the end of the voyage with files being between 15 and 25 MB.

2.4. Seismic reflection

The survey area was traversed by regional seismic reflection surveys starting in 1983. These data were downloaded from the Scientific Committee for Antarctic Research (SCAR) Seismic Data Library (https://sdls.ogs.trieste.it/cache/index.jsp) and loaded into Down Under Geosolutions *Insight* software (Fig. 2a).

On the survey, high resolution multichannel seismic lines were collected by the National Institute of Oceanography and Applied Geophysics (Italy) as part of the PNRA TYTAN project. These lines were collected using a 450 cu. Inch (7.37 l) GI gun array source and a 96 channel, 300 m hydrophone streamer. The shot spacing was 18.75 m.

Seismic sections were processed to stack sections. In this study, they are used to provide an overview of the sea floor landforms. Detailed interpretations are presented in Donda et al., 2020).

2.5. Sediment cores

The survey collected 11 kasten cores and 6 long piston cores. In this study, three piston cores and three kasten cores are discussed (Fig. 2a). Piston cores were logged for Magnetic susceptibility, and Natural Gamma radiation using a Malvern Multisensor core logger on the ship, then split, described and sampled on shore. Kasten cores were logged and sampled on recovery and channel samples taken for later use. These channel samples were logged for Magnetic susceptibility using a Bartington loop and point sensor.

In this study, cores are used for preliminary interpretation of depositional environments. Detailed analyses will be presented elsewhere.

2.6. Classification/mapping

The area features northeast-southwest trending canyons separated by topographic ridges. The canyons start on the upper slope then coalesce. To aid discussion, the main trunk canyons have been named using words provided by the indigenous people of the region of Australia that was adjacent to the Sabrina margin prior to continental rifting (Fig. 2b, c). These names have been submitted to the Standing Committee for Undersea Feature Names. Tributary canyons are named after the main canyon with numbers from west to east, for example, the western most tributary of Maadjit Canyon is named Maadjit 1. Ridges are named informally after the canyon or valley immediately to the east. For example, Minang-a Ridge is the ridge on the western side of Minang-a Canyon.

The various images and outputs were examined to map geomorphic

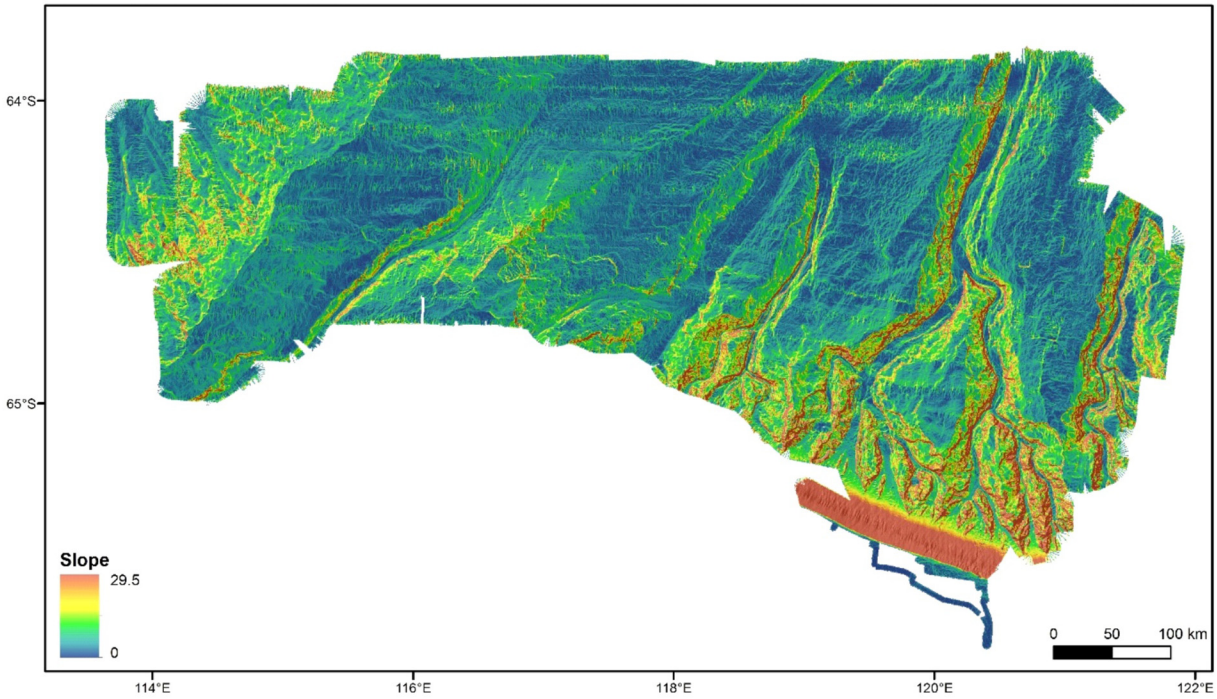

Fig. 5. Map of slope values derived from the multibeam raster using ArcGIS hydrological tools. Areas of orange to red are areas of high slope of which the steep upper slope region in the south eastern corner is the most prominent. (For interpretation of the references to colour in this figure legend, the reader is referred to the web version of this article.)

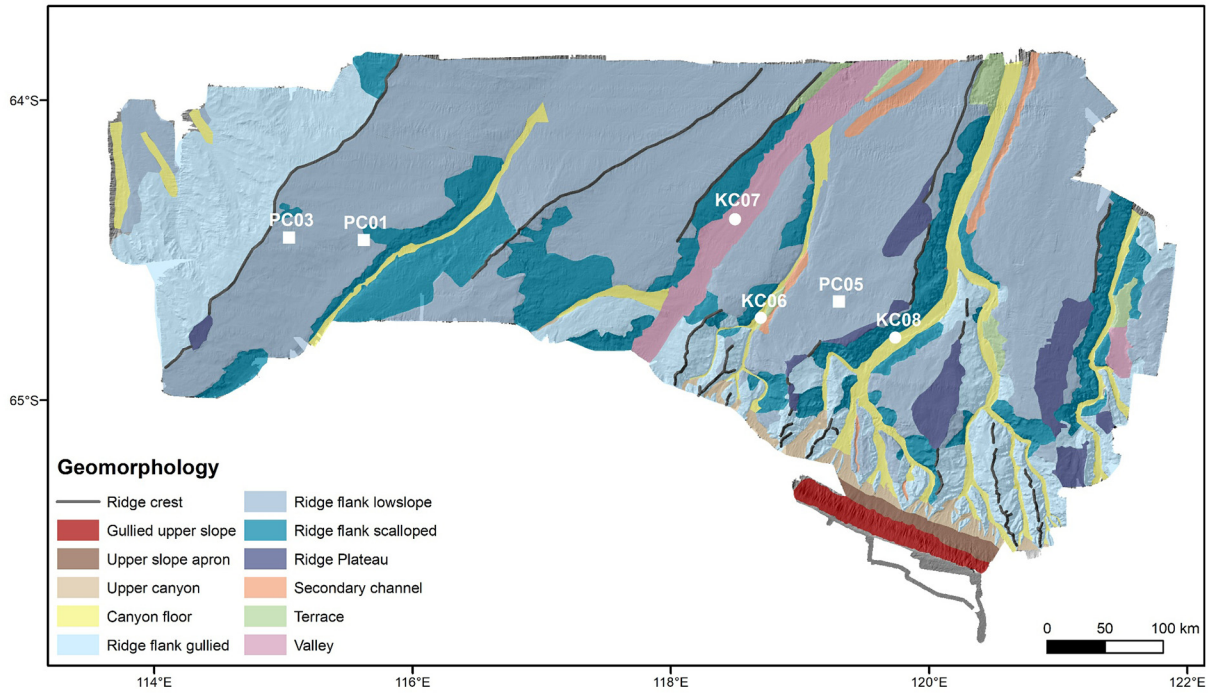

Fig. 6. Geomorphic classes mapped on Sabrina Coast slope and rise. The locations of sediment cores discussed are marked.

classes by hand tracing of polygon boundaries in ArcMAP (Fig. 6).

2.6.1. Canyon floor

Areas in canyons of relatively flat gradient in cross section. The upper extent is the lower edge of the upper canyon that contains smaller scale longitudinal ridges and bars (Fig. 7).

2.6.2. Valley

An area of relatively flat surface in cross section, gradually widening and deepening downslope, which lack obvious drainage features and major connections to the shelf and upper slope. The largest valley (Morka Valley) looks like a swale between ridges, though Jeffrey Canyon flows into it.

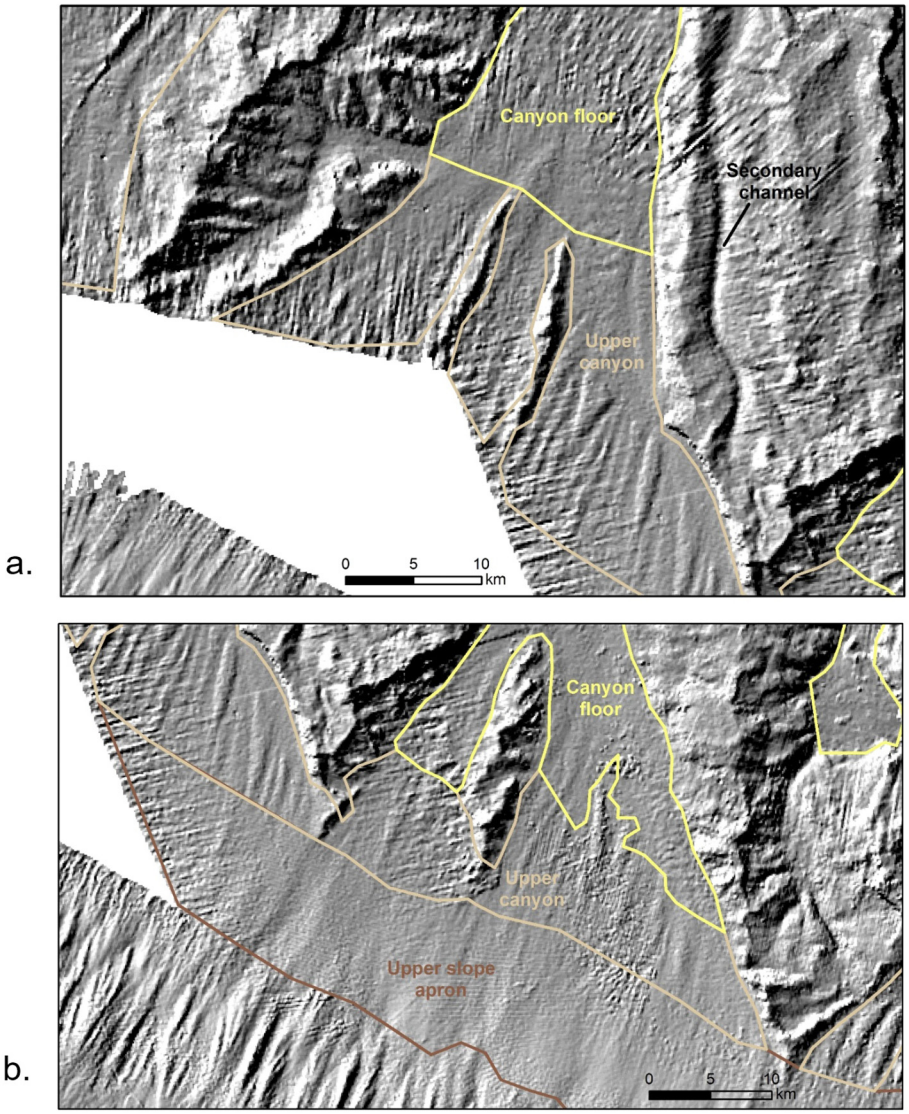

Fig. 7. Shaded images of bathymetry with class boundaries showing the Upper slope-Upper canyon-canyon boundaries. Fig. 7a also shows a secondary channel.

2.6.3. Upper canyon

Zone of narrow ridges and gullies upslope from larger ridges where the canyons narrow towards the main, and tributary canyons. The upslope limit is a band of smooth seafloor without ridges mapped as the Upper Slope Apron (Fig. 7).

2.6.4. Ridge

Elongate positive features where slope direction changes by around 180°. This feature is a set of lines that were mapped to identify the crest of individual ridges.

2.6.5. Ridge Plateau

Areas of very low slope on the crests of submarine ridges (Figs. 5, 6).

2.6.6. Ridge flank-Scalloped

Sloping sides of ridges with common scarps oriented roughly parallel to the ridge axis and canyon axis. Some scarps are clearly arcuate (Fig. 8). Scalloped ridge flanks show hummocky surfaces with common reversal of slopes.

2.6.7. Ridge flank-Gullied

Sloping sides of ridges with small channels oriented at a high angle to the ridge axis (Fig. 9). Some show a dendritic pattern. The orientation of these channels down the local slope suggests that they are cut by currents originating at the top of the local slope.

2.6.8. Ridge flank-low slope

Sloping sides of ridges with gently undulating surface lacking obvious channels or scarps.

2.6.9. Secondary channel

Areas that are morphologically channels but are separated from main canyons by steps (Hanging valleys). Their position in the landscape suggests they are canyon segments that have had their tributary areas captured by adjacent segments or, in downslope areas, are canyon segments abandoned by lateral shifts of the thalweg which has then entrenched (Fig. 7).

2.6.10. Terrace

Several canyons feature areas of flat to very gently sloping sea floor adjacent to the main canyon but at a shallower depth (Fig. 10a). Depth differences can be as much as 200 m and if sloping, the slope may be away from the canyon floor and downstream (Fig. 10b). A few terraces have low-relief hummocky surfaces.

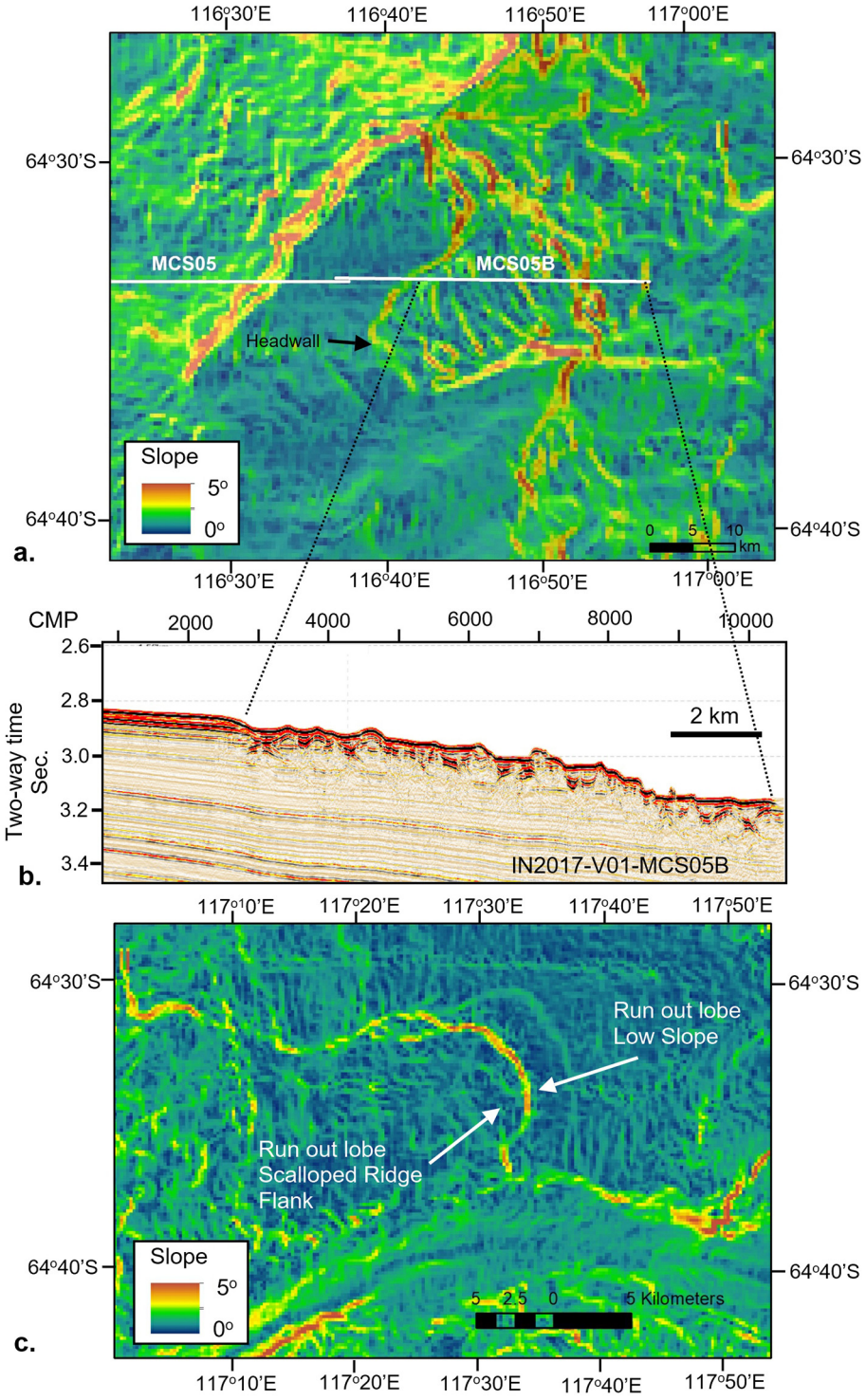

Fig. 8. a. Slope raster of multibeam data showing a well-developed slump feature as part of the Ridge Flank-Scalloped geomorphic class. The slump comprises a headwall and lateral sides. Within the body of the slump, crests of coherent slide blocks appear as steep linear to arcuate features parallel to the headwall. Location of seismic line shown. b. Seismic line crossing the slump obliquely. Undisturbed sediment next to the slump show a low slope sea floor and parallel reflectors. The slump shows coherent blocks which protrude above the general level of the slump surface. c. Slope raster of multibeam data showing run out lobes of slump debris visible in both Scalloped Ridge Flank and Low Slope Ridge Flanks.

2.6.11. Upper slope gullies

A zone of steep gullied slope extends from at or just below, the shelf edge at about 500 m depth to depths of around 1400–2200 m (Figs. 5, 6, 7).

2.6.12. Upper slope apron

Area of smooth seafloor on the upper slope formed by an apron of sediment deposited at the base of the upper slope gullies, and continuing until the slope reduces and downslope-oriented ridges emerge at around 2500 m (Fig. 7).

3. Results

The study area shows a clear distinction in the style of geomorphic features between the regions east of the Morka Valley and the region to the west.

3.1. Canyons

3.1.1. Overall geometry

The canyons of the Sabrina Coast slope and rise have low sinuosity, i.e. less than 1.2. Of the main canyons, only Boongorang and Manang

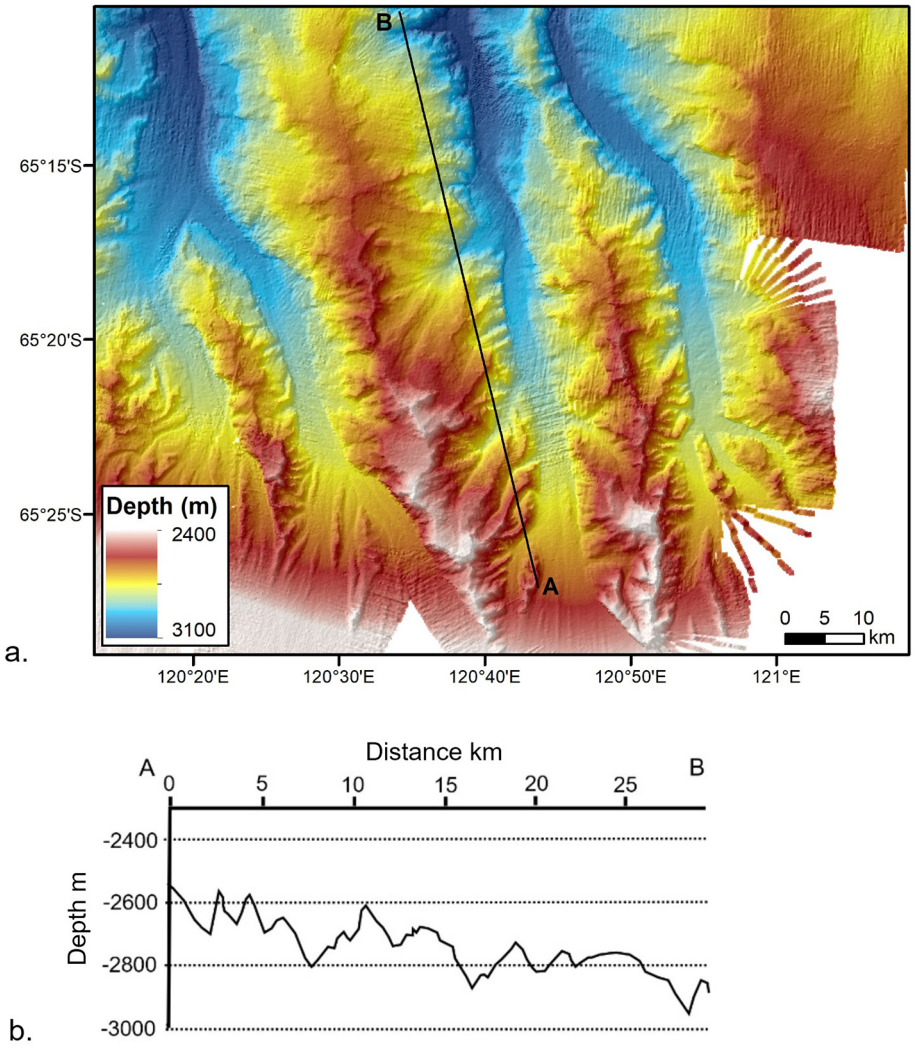

Fig. 9. Ridge Flank-Gullied. a. Map view. b. Profile A-B.

Canyons have sinuosities of greater than 1.1. The most sinuous part of any of the canyons is the western-most tributary of Maadjit Canyon (Maadjit 1) which displays a pronounced bend, initially flowing N then swinging towards the SE where it joins the main canyon (Fig. 11). This bend gives it a sinuosity of 1.46. The range of sinuosities is comparable to submarine channels and canyons fed by glacial sediments in the Gulf of Alaska but lower than other submarine channels (Shumaker et al., 2018).

Canyon long profiles are mostly concave up, catenary curves (Fig. 11), with local reverse slopes and mounds in a few places. The exception is Minang-a Canyon. It shows a straight to convex-up long profile over the 100 km mapped in this survey (Fig. 12).

Canyon Width-Depth ratios (Table 1) follow a basic pattern with high W/D in the headwater region (Upper Canyon) and again at the distal end of canyons that flow out on to the continental rise. Between the headwaters and distal zones, the Boongorang, Manang, Jeffrey and Minang-a canyons have W/D mostly in the range of 30 to 70, excluding zones of confluence between canyon tributaries. Maadjit Canyon has more variable W/D in its middle reaches. It reaches a maximum W/D of 91 in a segment which is a broad easterly curve with a terrace on the inner, easterly bank of the bend (Fig. 11). The other canyons do not feature such wide bends. The canyon with the most consistent W/D is Minang-a Canyon which has W/D between 48 and 85 for its entire length until broadening in a short segment at its distal end. Maadjit and Jeffrey Canyons broaden to a W/D of over 100 near their distal end, while Jeffrey Canyon broadens at its confluence with the Morka Valley and Maadjit Canyon on the continental rise. This widening reflects a loss of competence by turbidity currents at the distal end of canyons (Shumaker et al., 2018).

Canyon cross sections were analysed for their shape using the b coefficient that measures their tendency to V or U shapes (Pattyn and Van Huele, 1998). Most profiles are V shaped except for some distal reaches that are U shaped and some reaches that contain terraces and confluences of tributaries. Maadjit Canyon is commonly U shaped.

Subbottom profiler cross sections, show that canyons other than Minang-a, have steep walls with hummocky surfaces and flat to gently sloping floors with a narrow channel on one side. Subbottom acoustic penetration with reflectors are observed on gently sloping parts of canyon floors, particularly in areas further from the shelf break (Fig. 13). Minang-a Canyon shows a roughly symmetric cross-section with less steep valley sides than the canyons to the east (Fig. 14). Subbottom profiler lines show reflectors extending close to the canyon walls on most lines that cross perpendicular to the canyon with common small-scale steps and mounding, likely formed by slumping (Fig. 13).

3.1.2. *Upper canyon*

The Upper Canyon geomorphic unit is the transition zone between the upper slope apron and the region of clearly defined canyons and ridges. The Upper Canyon area features small ridges elongated

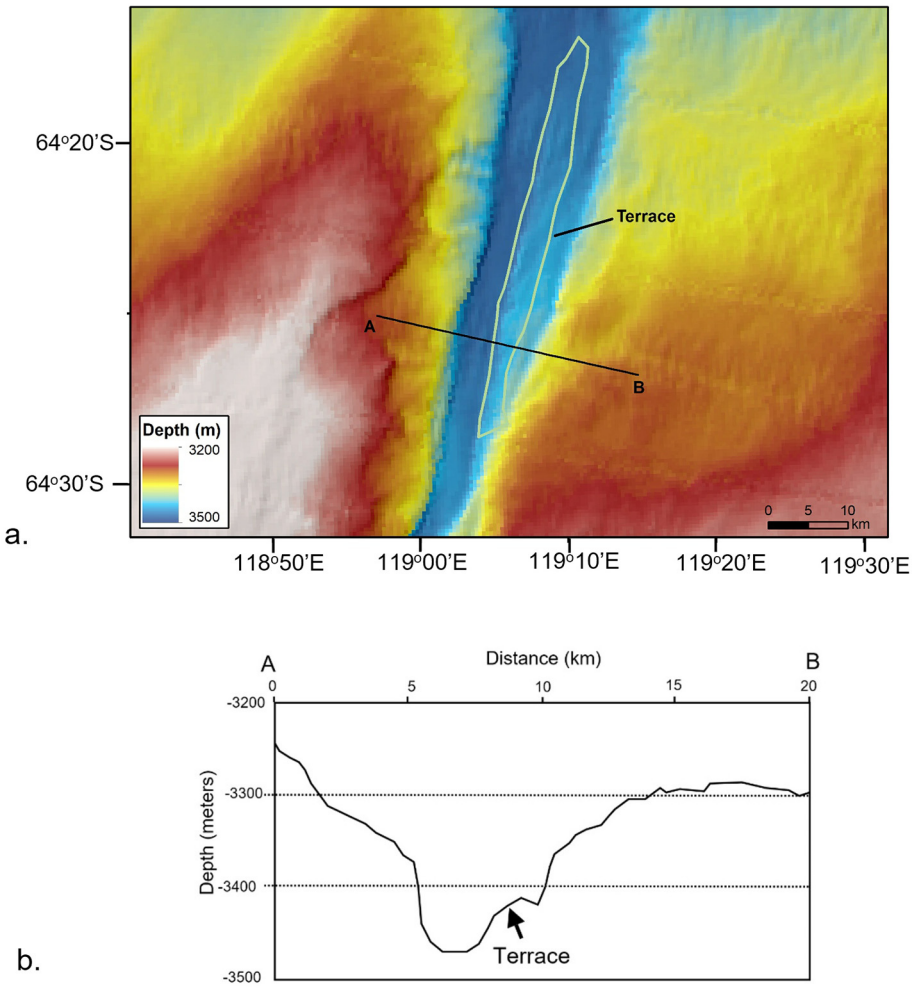

Fig. 10. a. Terrace within a submarine canyon. b. Bathymetric profile across a terrace and canyon showing the elevation difference between the canyon floor and the terrace.

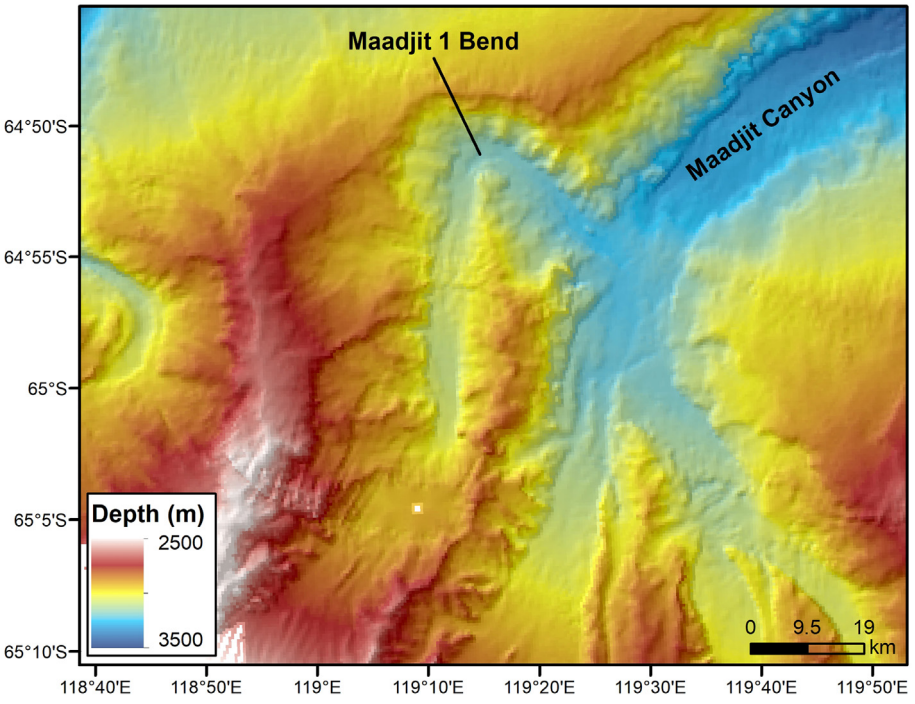

Fig. 11. Bend in the western most tributary (Maadjit 1) to Maadjit canyon.

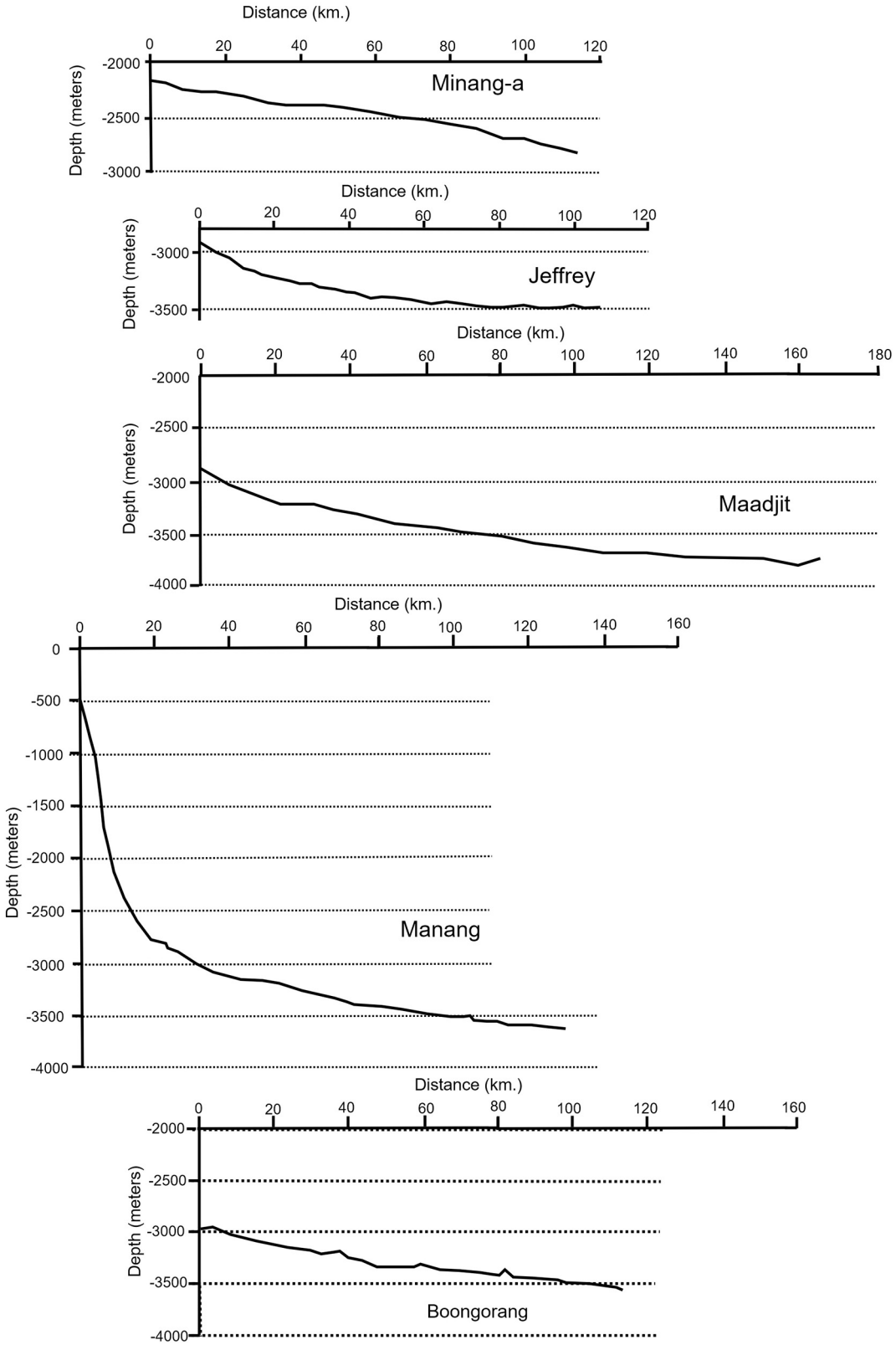

Fig. 12. Canyon thalwegs derived by tracing the deepest part of each canyon on the IN2017-V01 multibeam data. Only the Manang Canyon has multibeam data extending to the continental shelf edge. The other profiles are aligned so they start at approximately the distance the data starts from the shelf edge.

downslope. Subbottom profiles show no penetration suggesting hard sediment.

3.1.3. Terraces

Most of the terraces present along the sides of canyon floors are analogous to river terraces, formed by lateral migration of the channel thalweg, which then narrowed and entrenched. There is a large

Table 1
Width and depth ranges and W/D for canyons in the study area and for Morka Valley.

Canyon	Width Range (km)	Depth Range (m)	W/D (Mean)
Boongorang	6.7–28.5	166–318	34
Manang	6.37–22.38	113–465.6	44.6
Maadjit	5.3–9.5	72–159	77.5
Jeffrey	4.2–9	36–179	73.6
Minang-a	4.8–16	89–200	65.6
Morka Valley	13.2–17.5	59–166	179

(~150–200 m) elevation difference between some terraces and adjacent canyon floors. Terraces with hummocky surfaces are likely formed by local mass movement depositing slump material in the canyon, which has not yet been reworked by turbidity currents along the canyon axis.

3.1.4. Secondary channels

Secondary Channels suggest periods where canyons cut down at faster rates in different places so that some canyon reaches were captured, leaving segments of the network abandoned. Comparisons with fluvial systems suggest that canyons have gone through a period of aggradation followed by entrenchment by erosive but laterally restricted currents. Canyon reach capture represents an extreme consequence of axial incision described by Baztan et al. (2005).

3.2. Ridges

The ridges in the survey area displays distinct styles of morphology either side of Morka Valley. The differences are best illustrated by the seismic line RAE5108 (Fig. 15). East of Morka Valley, canyon ridges are asymmetric with steeper sides facing East. The Ridge crests are at depths of around 2800 m to 3400 m. Ridge crests are in the order of 30 to 40 km apart. West of the Morka Valley, the two ridges (Morka and Minang-a Ridges) can be viewed as part of a larger sediment body with a shallow canyon cut into it. The shallowest part is on the Minang-a Ridge where water depths less than 2000 m are common. Where the seaward end of the Morka and Minang-a Ridges are mapped by our multibeam data, they diminish to about 60 m high and 10s of kilometres across with steep sides facing east and gently sloping sides facing west.

3.2.1. Ridge plateaus

Ridge Plateaus are zones of very low slope on the crest of some ridges. Subbottom profiles show reflectors parallel to the sea bed. They represent areas of sediment accumulation that have been unaffected by mass movement or local currents. They occupy a small part of the study area (Fig. 6).

3.2.2. Ridge flank: Scalloped

Scalloped ridge flanks represent areas of sediment mass movement. The arcuate scarps characteristic of this geomorphic unit represents headwall scarps of slumps. The hummocky areas downslope of the scarps are slump deposits. Most such areas are chaotic without clearly

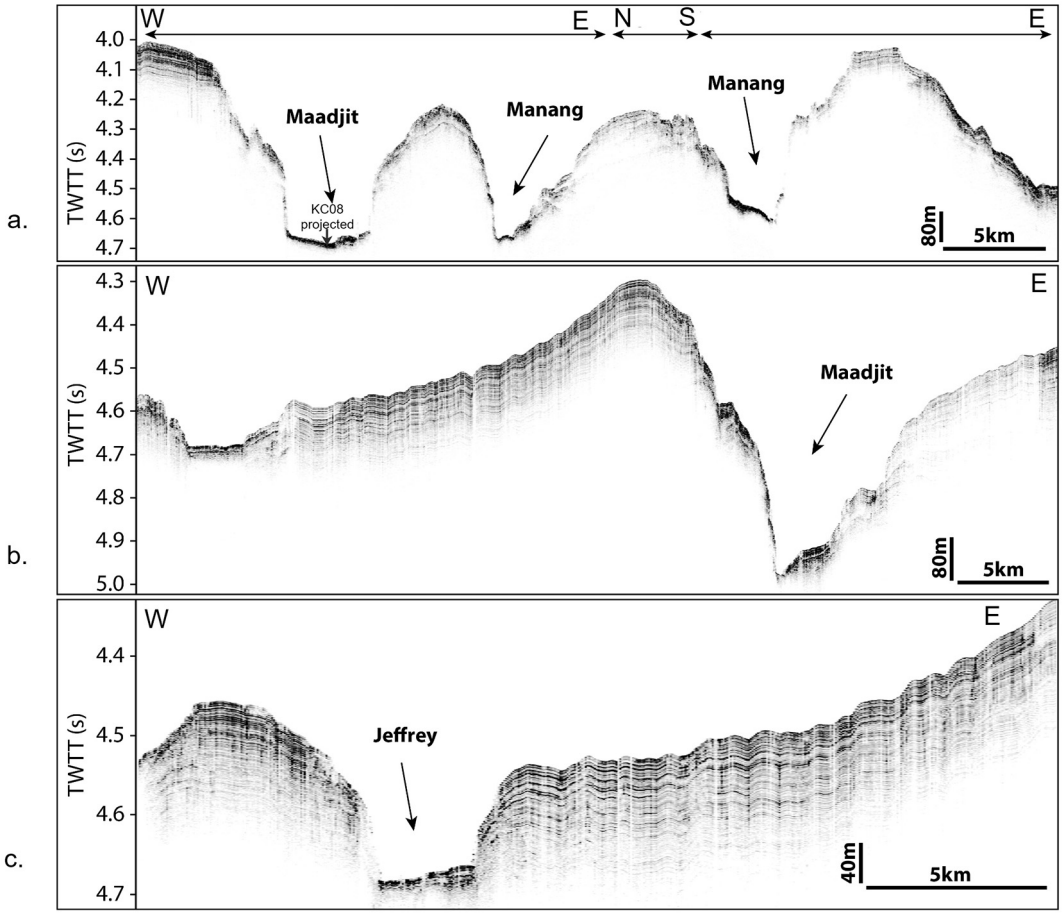

Fig. 13. Examples of canyon subbottom profiles. Profile locations shown on Fig. 2a. Vertical scale bar calculated using a sediment velocity of 1600 msec^{-1} (Stagg et al., 2004). a. Maadjit and Manang Canyons, upper reaches. Projected position of Kasten core KC08 shown. b. Maadjit Canyon, middle reach. c. Jeffrey Canyon, distal reach.

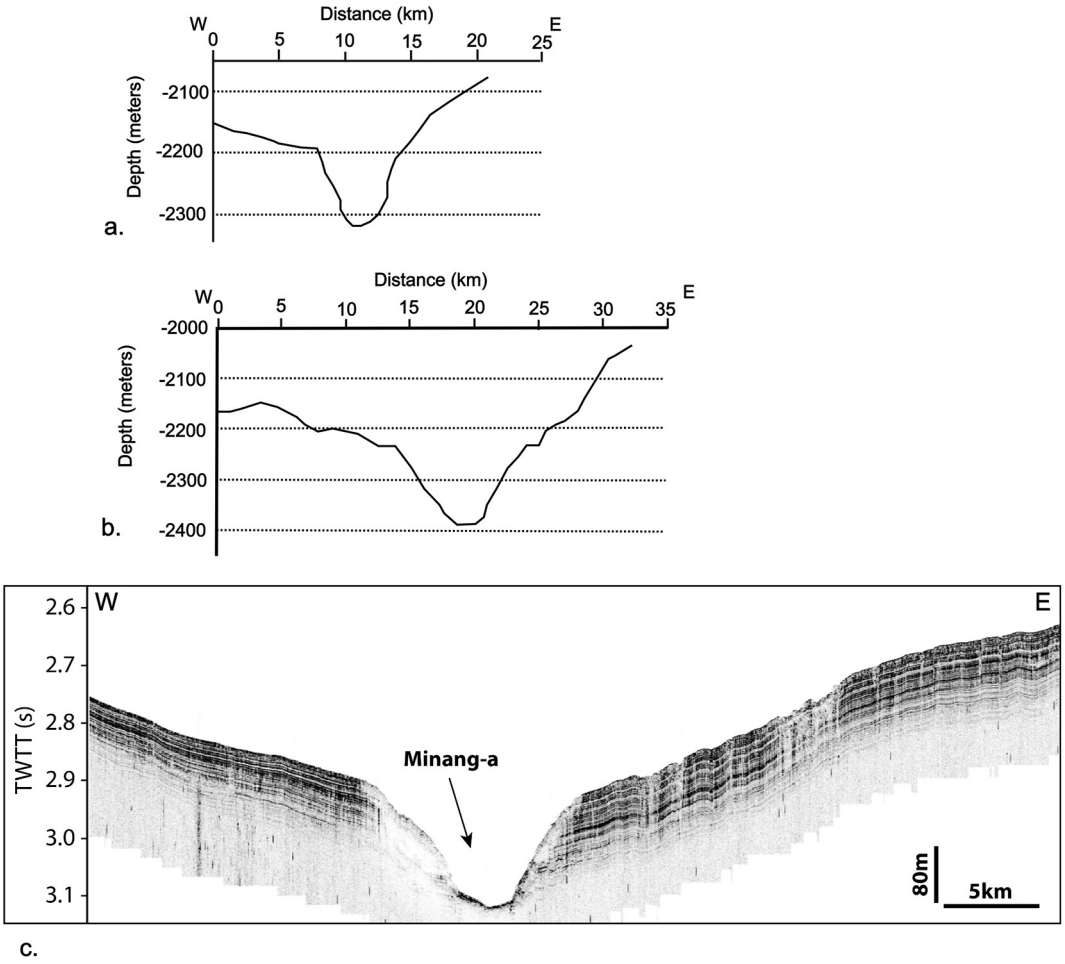

Fig. 14. a. Cross section normal to axis of Minang-a Canyon. b. Cross section normal to axis of Minang-a Canyon. c. Subbottom profile, Minang-a Canyon. Location shown on Fig. 2a. Vertical scale bar calculated using a sediment velocity of 1600 msec-1 (Stagg et al., 2004).

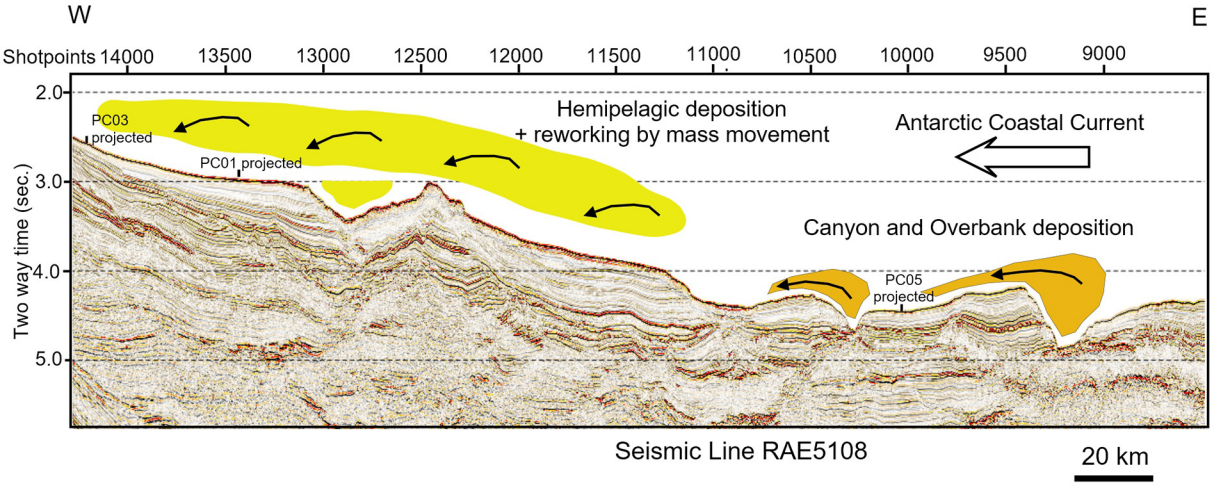

Fig. 15. Overview of the study area (Seismic line RAE5108). In the eastern part of the area, sediment lofted by turbidity currents advects west, building sediment ridges adjacent to the canyons. In the western part of the area, widespread sedimentation builds broad ridges. Slumping of ridge flanks feeds canyons. Projected locations of Piston cores PC01 and PC03 are shown.

visible slump features on subbottom profiles and seismic sections. However, there are some clearly visible slumps, such as on the east facing side of Morka Ridge (Fig. 8a). The shaded multibeam image shows an arcuate headwall and lateral ramps delineating the slump extensional zone, which features ridges roughly parallel to the headwall. These ridges are coherent, rotated blocks that have moved on a basal glide plane (Fig. 8b). In seismic and subbottom profiler sections, the ridge sediments upslope of the headwall display continuous, closely spaced reflectors (Fig. 8b) that change abruptly to a jumble of reflection-free blocks protruding above the rest of the sea floor. The slump

zone extends about 100 ms or 75 to 100 m below the sea floor (assuming a seismic velocity of 1800 msec^{-1}) suggesting a shallow décollement surface. This slump passes downslope into a zone of hummocky sea floor, which appears to be multiple, overlapping slump deposits so the individual run-out zone is hard to identify.

The hummocky surfaces and scarp orientations suggest these parts of the ridges are dominated by slumping. The scarps are likely headwalls and the hummocky surface caused by semi-coherent slide blocks and flows. The clearest examples of slumping on the eastern side of Boongorang Canyon and on Morka Ridge show arcuate headwalls, lateral scarps and ridges indicating rotated coherent slide blocks in the upper part of the slump (Fig. 8a). Morka and Minang-a Ridges also show convex-downslope ridges suggesting runout lobes of fluid debris originating from upslope slumps (Figs. 5, 8c).

3.2.3. Ridge flank: Gullied

Gullies on Gullied Ridge flanks are mostly v-shaped channels 100 m to 400 m across with up to 200 m of relief aligned parallel to the local slope (Fig. 9). Subbottom profiles show no penetration in these areas, though the steep, rough topography probably contributes to the lack of penetration. The spatial pattern of gullies and the grid-derived stream network shows that most gully systems are toe gullies in the terminology of Tubau et al. (2013) because they originate from the foot of the local slope, commonly the floor of a canyon, and do not commonly extend to the top of local slopes. An exception to this pattern is the western flank of Minang-a Ridge. There, some gullies originate at the break in slope on the western side of the ridge crest. They are rim gullies, though not originating at the shelf edge (Fig. 6).

3.2.4. Ridge flank – Low slope

Ridge flanks that display low slopes and subtle topographic variations are mapped together. Undulations suggest some processes reshaping the surface. The low slopes and height of features mean that they are hard to discern clearly without large vertical exaggeration, which also amplifies variations in the grid caused by noisy outer beams. The slope grid of the east- facing ridge flank of Morka Ridge shows subtle lobate features suggesting low profile debris flow run out lobes (Fig. 8c). The eastern side of Minang-a Ridge shows low-profile ridges and valleys with heights of between 40 and 50 m and widths of 8 to 10 km (Fig. 16). They trend roughly east-west and are slightly sinuous (Fig. 16). This pattern suggests shaping of the sea floor by currents but it is not clear whether these structures are formed by ocean currents flowing upslope or by sediment gravity flows moving downslope from the ridge crest. In some places, a map of Flow Accumulations shows some drainage systems extending from Gullied Ridge Flanks into areas of low slope.

The combination of features suggests the low slope ridge flanks represent areas of sediment accumulation which experience episodes of reworking by shallow mass movement and associated debris flows.

Subbottom profiles and seismic lines show well defined reflectors parallel to the sea floor over Ridge Plateaus and Low Slope Ridge Flanks (Figs. 13, 14, 15) indicating vertical accretion of sediment between canyons. The observation that the eastern sides of ridges are shallower and the sediment thicker indicate that significant amounts of sediment are deposited by spill over of turbidity currents from the canyons (Fig. 15). The Coriolis Effect and the Antarctic Coastal Current combine to displace the northward flowing turbidity currents to the West. Fine sediment is advected from the body of the currents so deposition is favoured on the Eastern side of each ridge, much in the way of a giant levee systems, although the scale of the ridges makes them better considered as a type of contourite deposit.

3.3. Valley

The Morka Valley differs from the submarine canyons on the Sabrina Coast Slope in having W/D ratios from 100 to 225, widening gradually downslope, a straight thalweg and a relatively flat floor (Fig. 17a). Its floor shows a prolonged subbottom profiler response but rare discernible reflectors. Morka Valley's sides feature mounded sea floor, mapped in most places as Scalloped Ridge Flank, though some areas are gullied. On seismic sections, the valley appears as a shallow trough containing sediment that onlaps its sides with the thickest part on the eastern side (Fig. 17b).

Morka Valley is likely not a submarine canyon but an elongate depression between two accreting ridges. It receives sediment from mass movement from the ridges and several submarine canyons but its straight thalweg suggests it is a sediment sink rather than a conduit for currents travelling to deeper water.

3.4. Core data

Most piston and kasten cores were taken from Ridge Plateau and Ridge Flank -Low Slope geomorphic classes. The depositional contexts for these cores are illustrated in Figs. 13, 15 and 17 by showing their projected positions on the subbottom profiles and seismic lines presented. The cores are dominated by silt, clay and diatomaceous clays with minor sand and occasional coarse grains. Most show well developed cycles of biogenic versus siliciclastic facies that are reflected in Magnetic Susceptibility and Natural Gamma log values. Such cycles have been shown to correlate with Marine Isotope Stages in many Antarctic sediment cores (Fig. 18a, e.g. Presti et al., 2011). This interpretation of the lithostratigraphy is supported by biostratigraphic analysis is in other publications (Holder et al., 2020). The cyclic sedimentation patterns suggest that the Ridge Plateau and Low Slope Ridge Flanks have received continuous fine sediment through the last 400,000 years, with diatom-rich deposition during interglacials and clay and silt rich intervals during glacial periods. Graded sand beds are absent indicating that the areas between canyons have not been affected by erosive turbidity currents. In contrast, piston core PC03 taken near the crest of the Minang-a Ridge, does not show this climate-related cyclicity (Figs. 2a, 18b). This core, while composed of the same sediment types as the others, contains evidence of current winnowing in the form of sharp bed boundaries, layers of sand grains and intraclasts. Its ridge-crest location suggests winnowing by the Antarctic Coastal Current.

Several attempts were made to collect kasten cores from the floors of the submarine canyons. Sites in Manang Canyon produced no sample and scratching of the core barrel suggests sand-rich sediment. Cores KC06 and KC08 in Jeffrey and Maadjit Canyons were successful and produced sections of clayey silts, silty clays and diatom bearing clays with some sandy laminae but also conspicuous diatomaceous intervals with laminated, mat-like to massive, clotted structure (Fig. 19). While there are no age models for these cores, these successions suggest that turbidity current activity in these canyons is confined only to parts of the climate cycle with fine and biogenic sediment accumulating in the canyon at other times. In both cores, over a meter of clay and silt rich sediments overlie the diatom mat/clotted intervals suggesting the diatom mats are not forming under present conditions.

One kasten core was taken in Morka Valley (KC07). It contains mostly clays, silts and diatom-rich clays, but also has sandy beds including graded clayey sands (Fig. 19). These facies suggest pelagic and hemipelagic sedimentation with episodes of turbidite deposition from currents formed by local slumping or from currents flowing down canyons that end in the valley (e.g. Jeffrey Canyon). At the time of writing, there was no age model for KC07.

4. Discussion

Almost all the canyons on the Sabrina Coast slope are typical of Antarctic canyons in showing a steep, smooth to gullied upper slope which then develops into larger gullies that coalesce into the canyons proper (Dowdeswell et al., 2006). This reflects a depositional regime

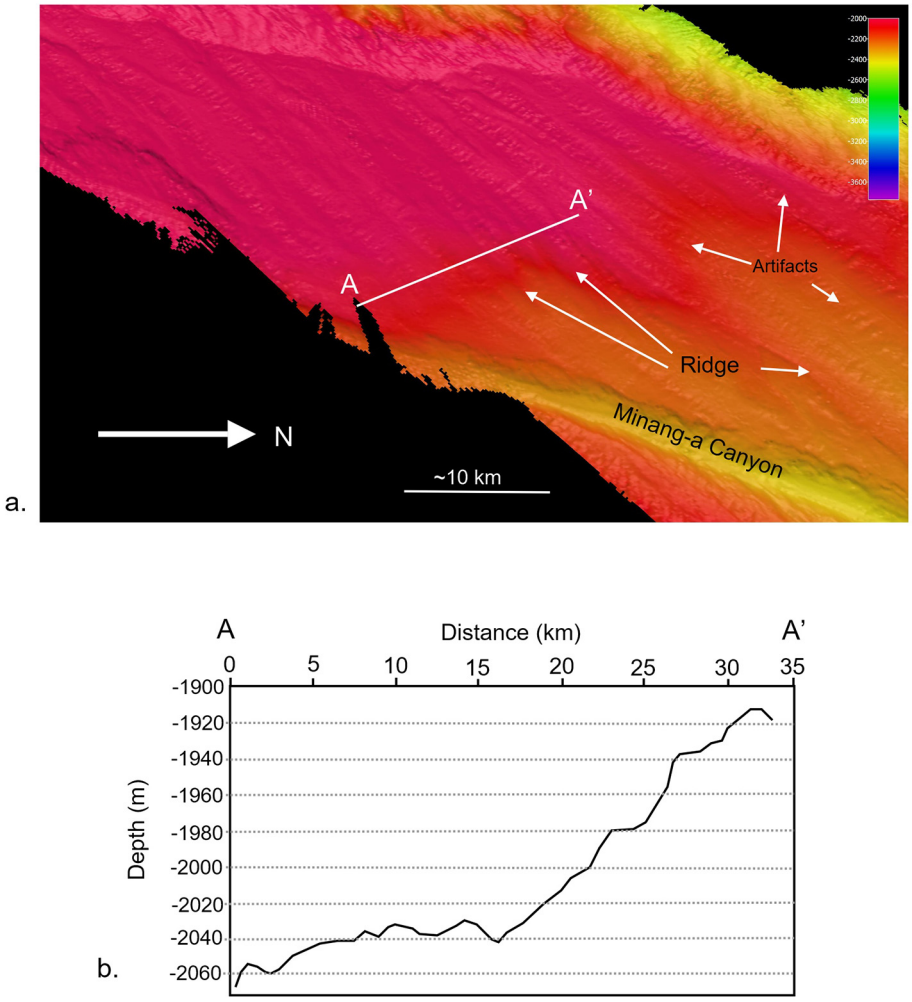

Fig. 16. Small scale ridges on Ridge Flank - low slope flanks on the western side of Minang-a Canyon. a. Fleidemaus image. b. Profile A-A' from multibeam bathymetry grid.

where abundant sediment is delivered to the shelf edge by grounded glacial ice (Gales et al., 2013). The canyons show terracing and small thalweg channels entrenched in the canyon floor. The terraces are not like those produced by channel migration described by Babonneau et al. (2010) but are more likely formed by episodes of deposition followed by axial incision (Baztan et al., 2005). This pattern of alternating erosion and deposition likely reflects the strong control exerted by climate cycles on the supply of sediment to the shelf edge. During glacial periods, the ice sheet advanced to points at or close to the shelf edge, delivering subglacial debris to the top of the slope. This sediment supply led to instability and slumping which generated turbidity currents on the upper slope (see Post et al., 2020) and in canyons. Protho et al. (2018) used core data from the Ross Sea to estimate that debris melts out from basal ice within about 1.2 km of the grounding zone but that sediment plumes carrying fine sediment can extend up to 250 km from the grounding zone. For this study area, these observations would see the highest level of activity and sand transport in canyons during peak glaciations when ice was at the shelf edge. The entire study area could have received fine sediment from meltwater plumes. Retreat of the ice from the shelf edge would have seen less coarse sediment transported down canyons but turbidity currents could still have been generated by slumping of sediment delivered by meltwater plumes. Ice retreat would have likely reduced the sediment supply and the frequency of mass movement and turbidity current generation. Once the ice retreated to the inner shelf, slope and rise sedimentation was dominated by biogenic sedimentation with lesser terrigenous sediment supplied by ice rafting and by iceberg scouring of the upper slope that could have contributed to less frequent mass movement. The dominance of biogenic sedimentation during interglacials is reflected in the kasten cores that recovered diatomaceous sediment from canyon floors.

This likely sequence of sedimentary processes would mean that most processes shaping the slope and rise geomorphology would be active during full glacial to stadial parts of the climate cycle. The development of pronounced ridges adjacent to the canyons is indicative of overbank deposition, with fine sediment lofted in the head and body of turbidity currents deposited on the ridges.

Deposition was greatest on the western side of the canyons due to displacement of the northward flowing turbidity currents by the combined effects of the Coriolis Effect and the Antarctic Coastal Current (Fig. 15). Active turbidity currents in the canyons would undercut canyon walls, forming toe gullies if slumping was small scale or larger rotational slumps that form Scalloped Ridge flanks.

The range of depositional geometries shown by the Sabrina Coast slope has many similarities to other studied areas of slope around the Antarctic. The large ridges on the western side of the area (Morka and Minang-a Ridges) display many of the features of ridges on the west Antarctic Peninsula margin described by McGinniss and Hayes (1995), Rebesco et al. (1996) and Amblas and Canals (2016). Both the Antarctic Peninsula (Mounds 6 and 7 of Rebesco et al., 1996) and the Morka and Minang-a Ridges show gently sloping sides facing up-current with the western-most, down-current side steeper with abundant gullies. These ridges are interpreted as contourites formed by re-distribution of

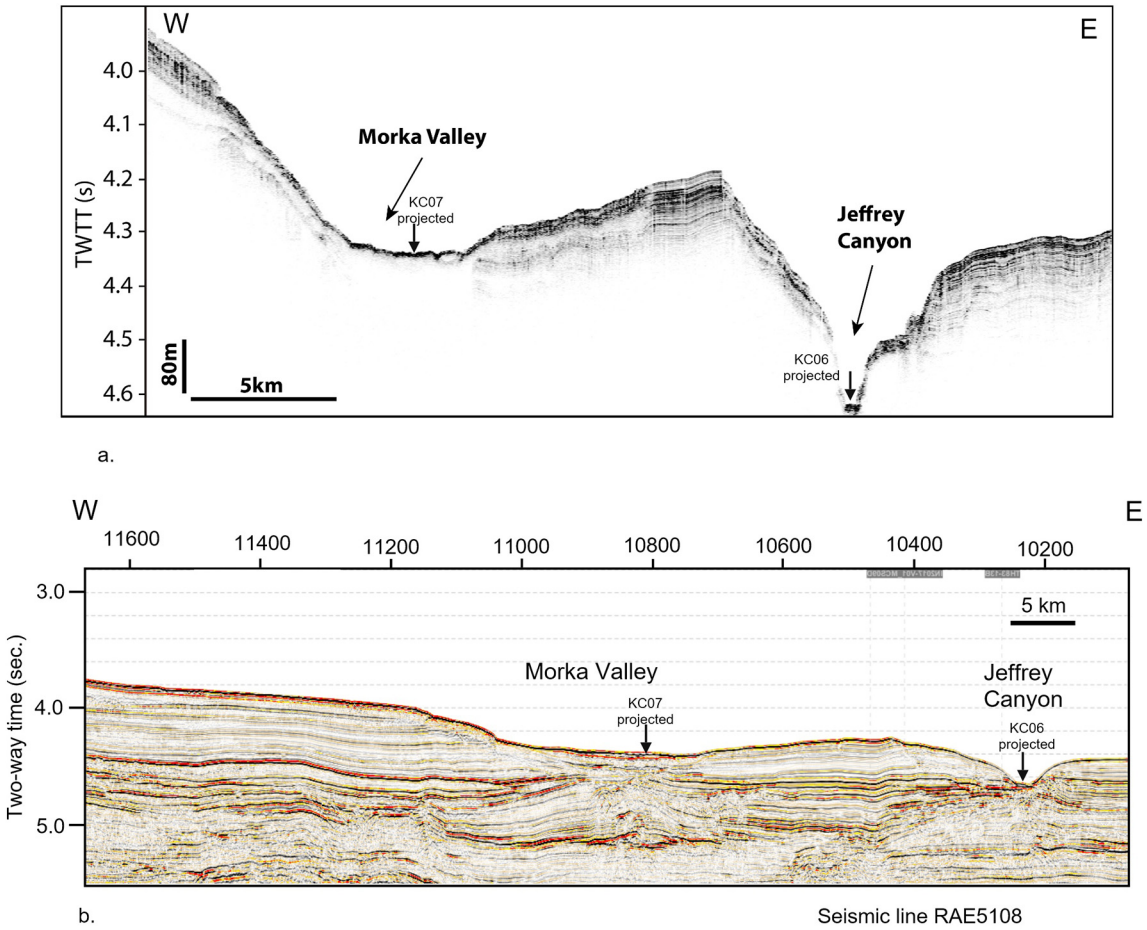

Fig. 17. a. Subbottom profile crossing Morka Valley and Jeffrey Canyon. Location shown in Fig. 2a. Vertical scale bar calculated using a sediment velocity of 1600 msec^{-1} (Stagg et al., 2004). The profile shows the difference between Morka Valley with its high W/D and a submarine canyon. Projected positions of Kasten cores KC06 and KC07 are shown. b. Seismic across Morka valley. Seismic line RAE5108.

detritus delivered to the slope by the Antarctic Coastal Current. The location of the Morka and Minang-a Ridges corresponds to the location of a cyclonic gyre identified by Wakatsuchi and Ohshima (1994). While the gyre may account for the recent deposition of contourites in this area, Wakatsuchi and Ohshima (1994) attribute the gyre to the presence of the ridges, suggesting the gyre came after the ridges formed. Further studies of seismic data will be needed to document the evolution of sedimentary processes and understand the role of different factors contributing to ridge formation. Another factor that is common to Mounds 6 and 7 on the Antarctic Peninsula margin and the Morka and Minag-a Ridges is that they are located seaward of outlet glaciers which may have a role in providing abundant suspended sediment to promote ridge growth.

Adams and Schlager (2000) described a range of canyon profiles from multiple margins and attributed the concave up, exponential curve of the sea floor to exponential decay of transport capacity downslope. They attributed deviations from this style of curve to variations in sea floor composition and along-slope transport of sediment. The Sabrina Coast canyon for which we have bathymetry from the shelf edge to its middle reaches, the Manang Canyon (Fig. 12), gives the clearest illustration of the exponential profile.

Morka and Minang-a Ridges differ from similar Antarctic slope-rise ridge complexes in that they extend far from the shelf edge (270 km), are oriented at an angle to the general trend of the continental margin and are separated by an unusual canyon, the Minang-a Canyon. Its thalweg differs from the other Sabrina Coast canyons and from many canyon profiles described in the literature in that it is convex (Fig. 12). Because of persistent sea ice, there are no bathymetric data south of the limit of our multibeam so it is difficult to assess the relationship between the Minang-a Canyon and the shelf edge. We suggest that the differences between the Minang-a Canyon and others stems from it being formed by mass movement which created turbidity currents at multiple points along the canyon sides. This is in contrast to the other canyons that are dominated by turbidity currents originating at the shelf break and upper slope, which transport sediment most of the length of the canyon. Turbidity currents formed by slumping of the canyon walls vary in competence along the canyon, causing variable deposition and erosion along the canyon length rather than steadily declining with distance from the shelf. The large ridges adjacent to the Minang-a Canyon form mostly from hemipelagic and contouritic deposition so the area receives a wide, relatively even spread of sediment from the water column. Then mass movement generates turbidity currents at many places along the ridge flanks, rather than mostly at the shelf edge and upper slope.

A further factor contributing to the convex thalweg of the Minang-a Canyon could be the presence of a trough mouth fan at the shelf edge that traps much of the coarser sediment transported by the Totten Glacier, as suggested by multibeam data described by Nitsche et al. (2017). These data suggest the shelf edge swings smoothly to be more east-west and deepens as it approaches the longitude of the Totten Glacier so a trough mouth fan could be present. Trough mouth fans can capture subglacialy transported sediment on the upper slope (Vorren and Laberg, 1997) and would trap coarse sediment from the Totten Glacier, making energetic turbidity currents travelling from the shelf edge to the distal end of the canyon rare. Other area of the Antarctic margin with similar sediment ridges mostly have canyons sourced from

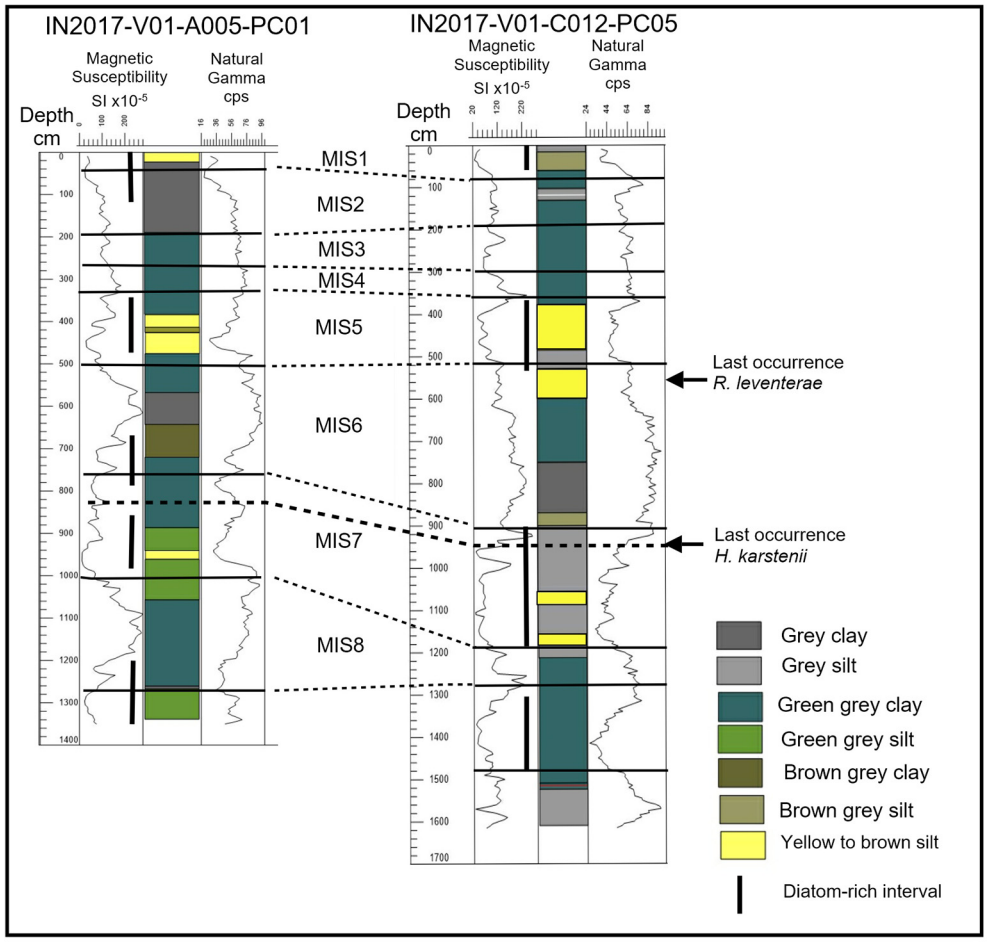

a.

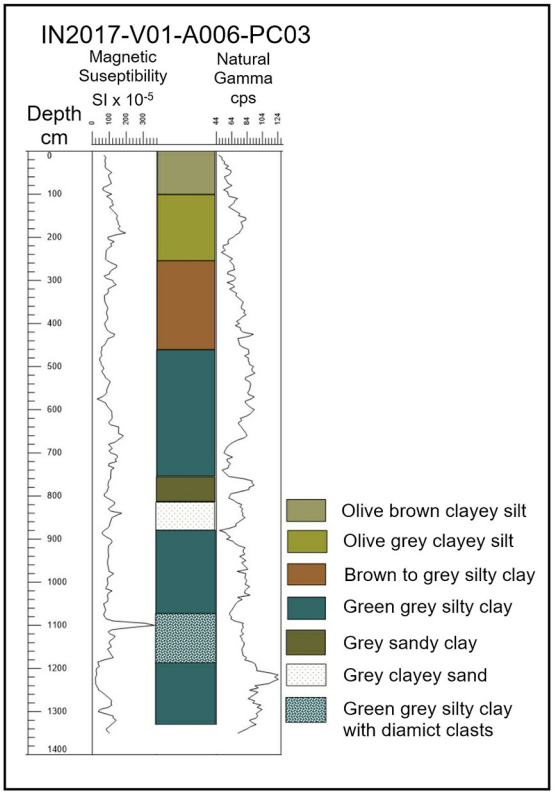

b.

Fig. 18. Generalised lithology and geophysical logs for piston cores from the study area. a. Core IN2017-A005-PC01 from a ridge in the western part of the study area and core IN2017-V01-C012-PC05 from a ridge between canyon in the east with preliminary correlation of Marine Isotope stages between them. Two diatom Last Occurrences are also marked. *H. Karstenii* last occurrence is just before the MIS7-MIS6 boundary and *R. leventerae* has a last occurrence just below the MIS6-MIS5 boundary. Piston core locations on Fig. 2a. Magnetic Susceptibility units are Volume Susceptibility (k) and Natural Gamma units in Counts per second (cps). b. Core IN2017-V01-A006-PC03 from a ridge crest on the western edge of the study area. Both Magnetic Susceptibility and Natural Gamma logs lack the fluctuations that indicate sedimentary cycles related to climate cycles and the sediments include facies including clayey sand beds and a bed of silty clay containing clasts of diamict that suggest reworking by currents or mass movement.

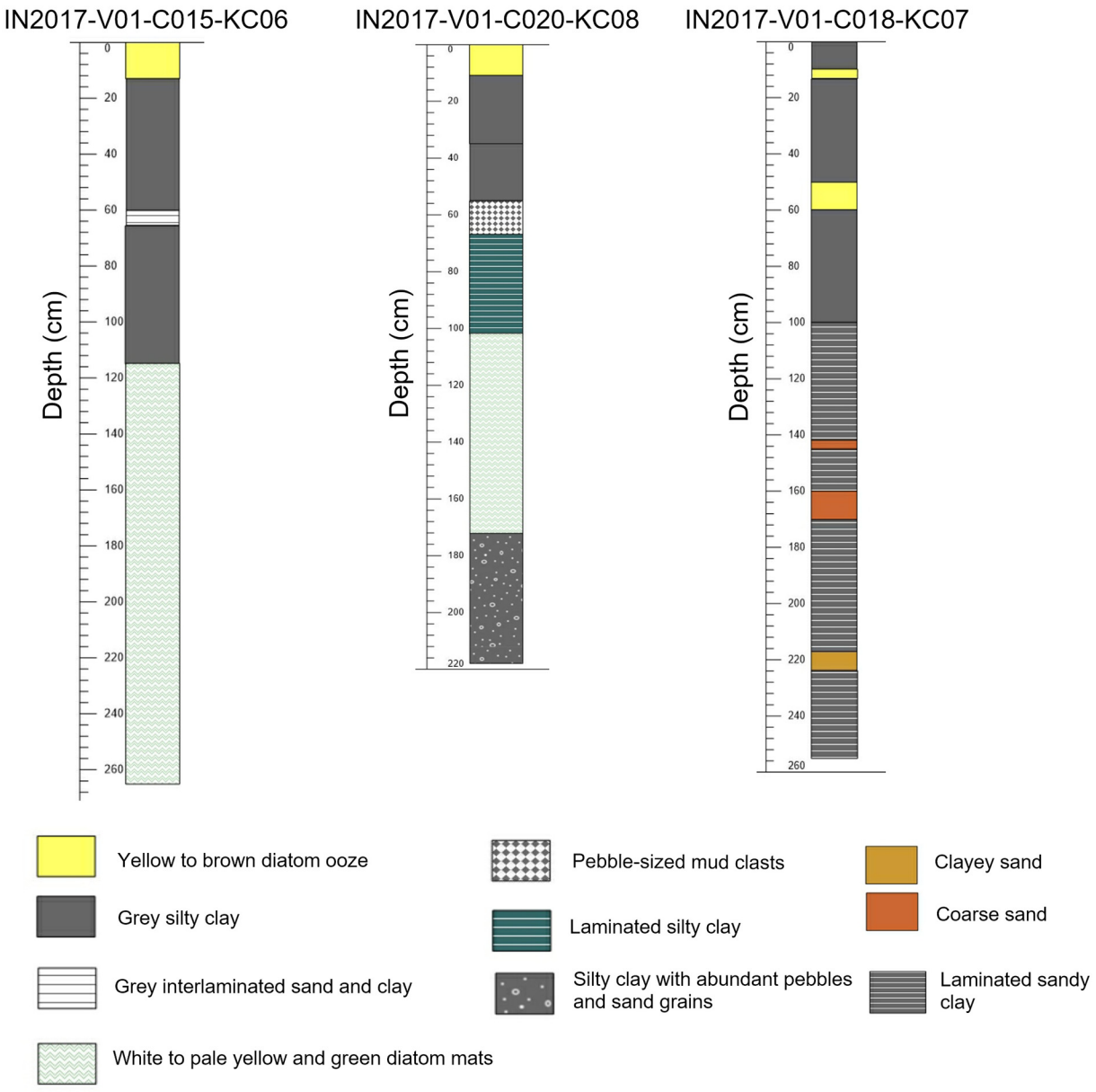

Fig. 19. Three Kasten cores from the study area. IN2017-V01-C015-KC06 was taken in the floor of Jeffrey Canyon, IN2017-V01-C020-KC08 from the floor of Maadjit Canyon and show diatom mat deposits. IN2017-V01-C018-KC07 was taken from the floor of Morka Valley. Locations are shown on Fig. 2a.

the upper slope (Amblas and Canals, 2016; Larter et al., 2016). The only possible example of a canyon similar to Minang-a Canyon set within a ridge flank is seen in Fig. 1b of Amblas and Canals (2016) where a canyon is present on the South-west flank of Drift 1, feeding the North Anvers Channel.

(Rebesco et al., 1997, Rebesco et al., 2002) proposed a model of contourite ridge formation for the Antarctic Peninsula that emphasised sediment supply from adjacent canyons. The Minang-a and Morka Ridges however seem derived from a widespread plume of sediment moving along the margin. The sediment plumes extending 250 km from the ice grounding line identified by Protho et al. (2018) were likely prime contributors to these ridges. Therefore, similar ridges might be expected on other glaciated margins although Rasmussen et al. (2003) concluded that strong contour currents would produce different ridge geometry. Thus, these ridges formed by the accretion on the gently sloping, up-current side, require a particular combination of abundant fine sediment and contour current strength.

5. Conclusions

The geomorphology of the Sabrina Coast Slope indicates that it is part of a continuum of mixed contourite-turbidite systems identified on the Antarctic margin (Kuvaas and Leitchenkov, 1992, Rebesco et al., 1996). In the eastern part of the study area, the ridges between canyons are clearly tied to their adjoining canyons and formed by westward advection of fine sediment lofted from turbidity currents and deposition of pelagic sediment. Canyons show evidence of sediment transport on their beds and erosion producing terraces and abandoned channels. The western part of the study area has ridges formed from a higher input from of sediment transported along the slope with their associated canyon not receiving a high proportion of turbidity currents that originate at the shelf edge, rather being fed by flows derived from slumping on the adjacent ridge flanks. Such a canyon derived entirely from its adjacent ridge is unusual in published data from the Antarctic margin. The ridges show a particular geometry with deposition on their gently-sloping, up-current side that reflects a high suspended sediment

supply and low contour current strength. These ridges formed with significant input of detritus from the East Antarctic ice drainage basins that feed Totten Glacier, making them prime locations to sample for sedimentary records of the history of this potentially sensitive part of the East Antarctic Ice Sheet. Other areas seaward of major outlet glaciers such as the slope off Prydz Bay may show a similar depositional regime (Kuvaas and Leitchenkov, 1992).

Declaration of Competing Interest

The authors declare that they have no known competing financial interests or personal relationships that could have appeared to influence the work reported in this paper.

Acknowledgments

We thank the Marine National Facility, the IN2017-V01 scientific party-led by the Chief Scientists L.K. Armand and P. E. O'Brien, MNF support staff and ASP crew members led by Capt. M. Watson for their help and support on board the *RV Investigator*. We thank laboratory staff from Geoscience Australia for sediment grainsize analysis, particularly Ian Long, Christian Thun, Aziah Williamson and Simon Webber. This Project is supported through funding from the Australian Government's Australian Antarctic Science Grant Program (AAS #4333) and by the Australian Government through the Australian Research Council (DP170100557). Seismic data acquisition and processing was supported by the Italian Programma Nazionale di Richerch in Antartide (PNRA) under the TYTAN Project. A. López-Quirós and D. Evangelinos acknowledge funding provided by Spanish Ministry of Science and Innovation (grants CTM2014-60451-C2-1-P and CTM2017-89711-C2-1-P). A. Post publishes with the permission of the CEO, Geoscience Australia, under Creative Commons. We also thank the anonymous reviewers for their comments.

References

Adams W., E., Schlager, W., 2000. Basic types of submarine slope curvature. J. Sediment. Res. 70 (4), 814–828.

Aitken, A.R.A., Roberts, J.L., van Ommen, T.D., Young, D.A., Golledge, N.R., Greenbaum, J.S., Blankenship, D.D., Siegert, M.J., 2016. Repeated large-scale retreat and advance of Totten Glacier indicated by inland bed erosion. Nature 533, 385–389.

Amblas, D., Canals, M., 2016. Contourite drifts and canyon-channel systems in the Northern Antarctic Peninsula Pacific margin. In: Dowdeswell, J.A., Canals, M., Jakobsson, M., Todd, B.J., Dowdeswell, E.K., Hogan, K.A. (Eds.), Atlas of Submarine Glacial Landforms: Modern, Quaternary and Ancient, Geological Society of London, Memoir. 46. pp. 393–394.

Armand, L.K., O'Brien, P.E., Party, On-board Scientific, 2018. Interactions of the Totten Glacier with the Southern Ocean through multiple glacial cycles (IN2017-V01). In: Post-Survey Report. Research School of Earth Sciences, Australian National University, Canberra. https://doi.org/10.4225/13/5acea64c48693.

Arndt, J.E., Schenke, H.W., Jakobsson, M., Nitsche, F.O., Buys, G., Goleby, B., Rebesco, M., Bohoyo, F., Hong, J., Black, J., Greku, R., Udintsev, G., Barrios, F., Reynoso-Peralta, W., Taisei, M., Wigley, R., 2013. The International Bathymetric Chart of the Southern Ocean (IBSCO) Version 1.0-a new bathymetric compilation covering circum-Antarctic waters. Geophys. Res. Lett. 40 (12), 3111–3117.

Babonneau, N., Savoye, B., Cremer, M., Bez, M., 2010. Sedimentary architecture in meanders of a submarine channel: detailed study of the present Congo Turbidite Channel (Zaiango Project). J. Sediment. Res. 80, 852–866.

Baztan, J., Berné, S., Olivet, J.-L., Rabineau, M., Aslanian, D., Gaudin, M., Réhault, J,-P. and Canals, M., 2005. Axial Incision: the key to understand submarine canyon evolution (in the western Gulf of Lion). Mar. Pet. Geol. 22, 805–826.

Beaman J., R., O'Brien E., P., Post L., A., De Santis, L., 2011. A new high resolution bathymetric model for the Terra Adelie and George V continental margin, East Antarctica. Antarctic Science 23, 95–103. https://doi.org/10.1017/S095410201000074X.

Bindoff, N.L., Rosenberg, M.A., Warner, M.J., 2000. On the circulation and water masses over the Antarctic continental slope and rise between 80 and 150° E. Deep-Sea Res. II 47, 2299–2326.

Close, D.I., Stagg, H.M.J., O'Brien, P.E., 2007. Seismic stratigraphy and sediment distribution on the Wilkes Land and Terre Adelie margins, East Antarctica. Mar. Geol. 239, 33–57.

Cooper, A.K., O'Brien, P.E., 2004. Leg 188 synthesis: Transitions in the glacial history of the Prydz Bay region, East Antarctica, from ODP drilling. In: Cooper, A.K., O'Brien, P.E., Richter, C. (Eds.), Proc. ODP, Sci. Results, 188 [Online], Available from World Wide Web. http://www-odp.tamu.edu/publications/188_SR/synth/synth.htm.

Donda, F., Brancolini, G., O'Brien, P.E., De Santis, L., Escutia, C., 2007. Sedimentary processes in the Wilkes Land margin: a record of Cenozoic East Antarctic Ice Sheet evolution. J. Geol. Soc. Lond. 164, 243–256.

Donda, F., Leitchenkov, G., Brancolini, G., Romeo, R., De Santis, L., Escutia, C., O'Brien, P., Armand, L., Caburlotto, A., Cotterle, D., 2020. The influence of the Totten Glacier on the distal sedimentary record: implications for the dynamics of the East Antarctic Ice Sheet during the Late Cenozoic. Antarct. Sci. https://doi.org/10.1017/S0954102020000188.

Dowdeswell A., J., Evans, J., O'Cofaigh, C., Anderson B., J., 2006. Morphology and sedimentary processes on the continental slope off Pine Island Bay, Amundsen Sea, West Antarctica. Bullet. Geolog. Soc. America 118, 606–619.

Escutia, C., Eittreim L., S., Cooper K., A., Nelson H., C., 2000. Morphology and acoustic character of the Antarctic Wilkes Land turbidite systems: ice -sheet-sourced versus river-sourced fans. J. Sediment. Res. 70 (1), 84–93.

Fernandez, R., Gulick, S., Domack, E., Montelli, A., Leventer, A., Shevenell, A., Fredrick, B., NBP1402 Science Party, 2018. Past ice stream and ice sheet changes on the continental shelf off the Sabrina Coast, East Antarctica. Geomorphology 317, 10–22.

Fonnesu, M., Palermo, D., Galiati, M., Marchesini, M., Bonamini, E., Bendias, D., 2020. A new world-class deep-water play-type, deposited by the syndepositional interaction of turbidity flow and bottom currents: the giant Eocene Coral Field in northern Mozambique. Mar. Pet. Geol. 111, 179–201. https://doi.org/10.1016/j.marpetgeo.2019.07.047.

Fretwell, P., Pritchard, H.D., Vaughan, D.G., Bamber, J.L., Barrand, N.E., Bell, R., Bianchi, C., Bingham, R.G., Blankenship, D.D., Casassa, G., Catania, G., Callens, D., Conway, H., Cook, A.J., Corr, H.F.J., Damaske, D., Damm, V., Ferraccioli, F., Forsberg, R., Fujita, S., Gim, Y., Gogineni, P., Griggs, J.A., Hindmarsh, R.C.A., Holmlund, P., Holt, J.W., Jacobel, R.W., Jenkins, A., Jokat, W., Jordan, T., King, E.D., Kohler, J., Krabill, W., Riger-Kusk, M., Langley, K.A., Leitchenkov, G., Leuschen, C., Luyendyk, B.P., Matsuoka, K., Mouginot, J., Nitsche, F.O., Nogi, Y., Nost, O.A., Popov, S.V., Rignot, E., Rippin, D.M., Rivera, A., Roberts, J., Ross, N., Siegert, M.J., Smith, A.M., Steinhage, D., Studinger, M., Sun, B., Tinto, B.K., Welch, B.C., Wilson, D., Young, D.A., Xiangbin, C., Zirissotti, A., 2013. Bedmap2: improved ice bed, surface and thickness datasets for Antarctica. Cryosphere 7, 375–393.

Gales, J.A., Larter, R.D., Mitchell, N.C., Dowdeswell, J.A., 2013. Geomorphic signature of Antarctic submarine gullies: Implications for continental slope processes. Mar. Geol. 337, 112–124.

Greenbaum, J.S., Blankenship, D.D., Young, D.A., Richter, T.G., Roberts, J.L., Aitken, A.R.A., Legresy, B., Schroeder, D.M., Warner, R.C., van Ommen, T.D., Siegert, M.J., 2015. Ocean access to a cavity beneath the Totten Glacier in East Antarctica. Nat. Geosci. 8, 294–298.

Gwyther, D.E., Galton-Fenzi, B.K., Hunter, J.R., Roberts, J.L., 2014. Simulated melt rates for the Totten and Dalton Ice Shelves. Ocean Sci. 10, 267–279.

Holder, L., Duffy, M., Opdyke, B., Leventer, A., Post, A., O'Brien, P., Armand, L.K., 2020. Controls on the intensity and duration of late Pleistocene glacial cycles in the slope sediments seaward of the Totten Glacier, East Antarctica. Paleoceanography (in review).

Jenkins, A., Dutrieux, P., Jacobs, S.J., McPhail, S.D., Perrett, J., Webb, A.T., White, D., 2010. Observations beneath Pine Island Glacier in West Antarctica and implications for its retreat. Nat. Geosci. 3, 468–472.

Khazender, A., Schodlok, M.P., Fenty, I., Ligtenberg, S.R.M., Rignot, E., van den Broeke, M.R., 2013. Observed thinning of Totten Glacier linked to coastal polynya variability. Nat. Commun. https://doi.org/10.1038/ncomms3857.

Kuvaas, B., Leitchenkov,, G., 1992. Glaciomarine turbidite and current controlled deposits in Prydz Bay, Antarctica. Mar. Geol. 108, 365–381.

Larter, R.D., Hogan, K.A., Dowdeswell, J.A., 2016. Large sediment drifts on the upper continental rise west of the Antarctic Peninsula. In: Dowdeswell, J.A., Canals, M., Jakobsson, M., Todd, B.J., Dowdeswell, E.K., Hogan, K.A. (Eds.), Atlas of Submarine Glacial Landforms: Modern, Quaternary and Ancient, Geological Society of London, Memoir. 46. pp. 401–402.

Levy, R.H., Meyers, S.R., Naish, T.R., Golledge, N.R., McKay, R.M., Crampton, J.S., De Conto, R.M., De Santos, L., Florindo, F., Gasson, E.G.W., Harwood, D.M., Luyendyk, B.P., Powell, R.D., Clowes, C., Kulhanek, D.K., 2019. Antarctic ice-sheet sensitivity to obliquity forcing enhanced through ocean connections. Nat. Geosci. 12, 132–138.

Macintosh, A., Golledge, N., Domack, E., Dunbar, R., Leventer, A., White, D., Pollard, D., DeConto, R., Fink, D., Zwart, D., Gore, D., Lavoie, C., 2011. Retreat of the East Antarctic ice sheet during the last glacial termination. Nat. Geosci. 4, 195–202.

McGinniss, J.P., Hayes, D.E., 1995. The roles of downslope and along-slope depositional processes: Southern Antarctic Peninsula continental rise. In: Cooper, A.K., Barker, P.F., Brancolini, G. (Eds.), Geology and Seismic Stratigraphy of the Antarctic Margin. American Geophysical Union Antarctic Research Series 68. pp. 141–156.

Nitsche, F.O., Porter, D., Williams, G., Cougnon, E.A., Fraser, A.D., Correia, R., Guerrero, R., 2017. Bathymetric control of warm ocean water access along the East Antarctic margin. Geophys. Res. Lett. 44, 8936–8944.

O'Cofaigh, C., Dowdeswell, J.A., Evans, J., Larter, R.D., 2008. Geological constraints on Antarctic palaeo-ice-stream retreat. Earth Surf. Process. Landf. 33, 513–525.

Pattyn, F., Van Huele, W., 1998. Power law or power flaw? Earth Surf. Process. Landf. 23, 761–767.

Post, A.L., O'Brien, P.E., Edwards, S., Carroll, A.G., Malakoff, K., Armand, L.K., 2020. Upper slope processes and seafloor ecosystems on the Sabrina continental slope, East Antarctica. Mar. Geol. 422, 106091.

Presti, M., Loïc, B., Denis, D., Schmidt, S., De Santis, L., Crosta, X., 2011. Sediment delivery and depositional patterns off Adélie Land (East Antarctica) in relation to late Quaternary climatic cycles. Mar. Geol. 284, 96–113.

Pritchard, H.D., Ligtenberg, S.R.M., Fricker, H.A., Vaughan, D.G., van den Broeke, M.R., Padman, L., 2012. Antarctic ice-sheet loss driven by basal melting of ice shelves.

Nature 484, 502–505.
Protho, L.O., Simkins, L.M., Majewski, W., Anderson, J.B., 2018. Glacial retreat patterns and processes determined from integrated sedimentology and geomorphology records. Mar. Geol. 395, 104–119.
Rasmussen, S., Lykke-Andersen, H., Kuijpers, A., Troelstra, S.R., 2003. Post-Miocene sedimentation at the continental rise of Southeast Greenland: the interplay between turbidity and contour currents. Mar. Geol. 196, 37–52.
Rebesco, M., Camerlenghi, A., Volpi, V., Neagu, C., Accettella, D., Lindberg, B., Cova, A., Zigur, F., The MAGICO Party, 2007. Interaction of processes and importance of contourites: insights from the detailed morphology of sediment Drift 7, Antarctica. In: Viana R.A., Rebesco, M. (Eds.), Economic and palaeoceanographic significance of contourite deposits, Special Publication. 276. Geological Society, London, pp. 95–110.
Rebesco, M., Larter, R.D., Camerlenghi, A., Barker, P.F., 1996. Giant sediment drifts on the continental rise west of the Antarctic Peninsula. Geomarine Lett. 16, 65–75.
Rebesco, M, Pudsey J, C, Canals, M., Camerlenghi, A., Barker F., P., Estrada, F., Giorgetti, A., 2002. Sediment drifts and deep-sea channel systems, Antarctic Peninsula Pacific Margin. In: Deep-water contourite systems: Modern drifts and Ancient Series, seismic and sedimentary characteristics, Memoir. 22. Geological Society, London, pp. 353–371.
Rintoul, S.R., Silvano, A., Pena-Molino, B., van Wijk, E., Rosenberg, M., Greenbaum, J.S., Blankenship, D.D., 2016. Ocean heat drives rapid basal melt of the Totten Ice Shelf. Sci. Adv. 2 (12). https://doi.org/10.1126/sciadv.1601610. e1 601610.
Shumaker E., L., Jobe A., Z., Johnstone A., S., Pettinga A., L., Cai, D., Moody D., J., 2018. Controls on submarine channel-modifying processes identified through morphometric scaling relationships. Geosphere 14 (5), 2171–2187. https://doi.org/10.1130/GES01674.1.
Smith, J.A., Hillenbrand, C.-D., Kuhn, G., Larter, R.D., Graham, A.G.C., Ehrmann, W., Moreton, S.G., Forwick, M., 2011. Deglacial history of the West Antarctic Ice Sheet in the western Amundsen Sea Embayment. Quat. Sci. Rev. 30, 488–505.
Stagg, H.M.J., Colwell, J.B., Direen, N.G., O'Brien, P.E., Brown, B.J., Bernadell, G., Borissova, I., Carson, L., Close, D.B., 2004. Geological framework of the continental margin in the regions of the Australian Antarctic Territory. In: Geoscience Australia Record 2004/025, (373 pages).
Tubau, X., Lastras, G., Canals, M., Micallef, A., Amblas, D., 2013. Significance of the fine drainage pattern for submarine canyon evolution: the Foix Canyon System, Northwestern Mediterranean Sea. Geomorphology 184, 20–37. https://doi.org/10.1016/j.geomorph.2012.11.007.
Vorren, T.O., Laberg, J.S., 1997. Trough mouth fans – palaeoclimate and ice sheet monitors. Quat. Sci. Rev. 16, 865–881.
Wakatsuchi, M., Ohshima, K.I., 1994. Obervations of cyclonic eddies in the Indian Ocean sector of the Antarctic Divergence. J. Geophys. Res. 99 (C10), 20417–20426.
Weber, M.E., Clark, P.U., Ricken, W., Mitrovica, J.X., Hosteler, Kuhn, G., 2011. Interhemispheric ice-sheet synchronicity during the last glacial maximum. Science 334, 1265–1269.
Williams, G.D., Meijers, A.J.S., Poole, A., Mathiot, P., Tamura, T., Klocker, A., 2011. Late winter oceanography off the Sabrina and BANZARE coast (117-128oE), East Antarctica. Deep-Sea Res. II 58, 1194–1210.
Wright P., A., Young A., D., Roberts L., J., Schroeder M., D., Bamber L., J., Dowdeswell A., J., Young W., N., Le Brocq M., A., Warner C., R., Payne J., A., Blankenship D., D., van Ommen D., T., Siegert J., M., 2012. Evidence of a hydrological connection between the ice divide and ice sheet margin in the Aurora Subglacial Basin, East Antarctica. J. Geophy. Res. 117 (F01033). https://doi.org/10.1029/2011JF002066.
Young, D.A., Wright, A.P., Roberts, J.L., Warner, R.C., Young, N.W., Greenbaum, J.S., Schroeder, D.M., Holt, J.W., Sugden, D.E., Blankenship, D.D., Van Ommen, T.D., Seigert, M.J., 2011. A dynamic early East Antarctic Ice Sheet suggested by ice covered fjord landscapes. Nature 474, 72–75.
Zwally, H.J., Giovinetto, M.B., 2011. Overview and assessment of Antarctic Ice Sheet mass balance estimates: 1992-2009. Surv. Geophys. 32, 351–376.